

Accepted to ApJ

Identifying the young low-mass stars within 25 pc. I. Spectroscopic Observations¹

Evgenya Shkolnik²

*Department of Terrestrial Magnetism, Carnegie Institution of Washington, 5241 Broad
Branch Road, NW, Washington, DC 20015*

shkolnik@dtm.ciw.edu

Michael C. Liu³

*Institute for Astronomy, University of Hawaii at Manoa
2680 Woodlawn Drive, Honolulu, HI 96822*

mliu@ifa.hawaii.edu

and

I. Neill Reid

Space Telescope Science Institute, Baltimore, MD 21218

inr@stsci.edu

ABSTRACT

We have completed a high-resolution ($R \approx 60,000$) optical spectroscopic survey of 185 nearby M dwarfs identified using ROSAT data to select active, young objects with fractional X-ray luminosities comparable to or greater than Pleiades

¹Based on observations collected at the W. M. Keck Observatory and the Canada-France-Hawaii Telescope. The Keck Observatory is operated as a scientific partnership between the California Institute of Technology, the University of California, and NASA, and was made possible by the generous financial support of the W. M. Keck Foundation. The CFHT is operated by the National Research Council of Canada, the Centre National de la Recherche Scientifique of France, and the University of Hawaii.

²Carnegie Fellow

³Alfred P. Sloan Research Fellow

members. Our targets are drawn from the *NStars* 20-pc census and the *Moving-M* sample with distances determined from parallaxes or spectrophotometric relations. We limited our sample to 25 pc from the Sun, prior to correcting for pre-main sequence over-luminosity or binarity. Nearly half of the resulting M dwarfs are not present in the Gliese catalog and have no previously published spectral types. We identified 30 spectroscopic binaries (SBs) from the sample, which have strong X-ray emission due to tidal spin-up rather than youth. This is equivalent to a 16% spectroscopic binary fraction, with at most a handful of undiscovered SBs. We estimate upper limits on the age of the remaining M dwarfs using spectroscopic youth indicators such as surface gravity-sensitive indices (CaH and K I). We find that for a sample of field stars with no metallicity measurements, a single CaH gravity index may not be sufficient, as higher metallicities mimic lower gravity. This is demonstrated in a sub-sample of metal-rich RV standards, which appear to have low surface gravity as measured by the CaH index, yet show no other evidence of youth. We also use additional youth diagnostics such as lithium absorption and strong H α emission to set more stringent age limits. Eleven M dwarfs with no H α emission or absorption are likely old (>400 Myr) and were caught during an X-ray flare. We estimate that our final sample of the 144 youngest and nearest low-mass objects in the field is less than 300 Myr old, with 30% of them being younger than 150 Myr and 4 very young (\lesssim 10 Myr), representing a generally untapped and well-characterized resource of M dwarfs for intensive planet and disk searches.

Subject headings: Stars: activity, chromospheres, coronae, late-type, ages – Surveys: X-ray – Galaxy: solar neighborhood

1. Introduction

Observational studies of planet formation have been energized by the discovery of young (<100 Myr) solar-type stars close to Earth (e.g. Jeffries 1995; Webb et al. 1999; Montes et al. 2001), identified from multiple indicators of youth including chromospheric activity and strong X-ray. The combination of distances, proper motions, and radial velocities has allowed many of these stars to be kinematically linked to coeval moving groups (e.g., Zuckerman & Song 2004; Torres et al. 2008). These young moving groups (YMGs) are several times closer to Earth than the traditional well-studied star-forming regions such as Taurus and Orion (\sim 150–500 pc). More importantly, these groups have ages of \sim 10–100 Myr, a time period in stellar evolution that has largely been underrepresented in previous

studies. This is expected to be a key epoch for understanding planet formation, coinciding with the end of giant planet formation and the active phase of terrestrial planet formation (e.g. Mandell et al. 2007; Ida & Lin 2008).

While these YMGs have been a boon for observers, the current census has severe limitations — in particular, it is mostly restricted to the higher-mass (AFGK-type) stars and contains very few low-mass M dwarfs. This paucity is striking given that M dwarfs dominate the stellar mass function by number: roughly 3 out of 4 stars in a volume-limited sample of the solar neighborhood are M dwarfs (Reid et al. 1995; Bochanski et al. 2008). For instance, in the 12-Myr old β Pictoris moving group, 17 of the 44 identified members (Torres et al. 2006) are M dwarfs, whereas we would expect 75% based on the stellar mass function: \sim 60 M dwarfs are missing from this group’s known members.

The incompleteness in the current young low-mass census arises from a combination of two factors: (1) Young star searches to date have relied on optical catalogs for distances and/or proper motions, e.g., the Hipparcos and Tycho catalogs (Perryman & ESA 1997), the former limited to $V < 7$ with parallaxes, while the latter limited to $V < 7$ but without parallaxes. However, M dwarfs are optically faint and thus make a disproportionately small contribution to these catalogs. (2) Until very recently, the only all-sky surveys suited for finding X-ray active stars have been the ROSAT¹ catalogs (Voges et al. 1999, 2000), and since the X-ray luminosities of M dwarfs are \sim 10–300× lower than solar-type stars, ROSAT detections are mostly limited to the nearest, earliest-M stars (Figure 1).

Previous searches for young, X-ray-active, late-type stars focused on a satellite’s detection limits rather than a volume-limited sample. E.g. Riaz et al. (2006) collected low-resolution spectra of \approx 800 M dwarfs (M0 – M5) detected with ROSAT with photometric distances ranging from 3 to 750 pc. They determine their sample to be generally young since the measured coronal activity of most of the stars is higher than that of Hyades members (\sim 600 Myrs). Zickgraf et al. (2005) collected high-resolution spectra of 118 ROSAT-selected G, K and M stars extending out to 600 pc and from lithium measurements, estimate that 25% of their sample is near the age of the Pleiades (\sim 120 Myr). And more recently, Covey et al. (2008) published a catalog of 348 stars identified from correlating the Chandra X-ray Observatory’s archival data with the Sloan Digital Sky Survey (SDSS). Of these, 36 are newly identified M dwarfs with distances out to 1000 pc and a wide range of X-ray and H α luminosities.

The goal of this program is to identify the best possible M dwarf targets for direct

¹The Röntgensatellit (ROSAT) was a joint German, US and British X-ray observatory operational from 1990 to 1999.

imaging searches of extrasolar planets and circumstellar disks. This requires a young, well-characterized, and nearby sample. The proximity is an essential benefit for studies requiring high sensitivity as large distances limit both the linear resolution and available flux with which we can image planets and detect disks. Also, M dwarfs in principle could represent the most common and nearest to Earth hosts of planetary systems, and provide a potentially much larger population of targets than has been studied to date.

It is imperative that we add youth as a criterion to our M dwarf sample as planets cool and fade significantly between 10 Myr and 1 Gyr. For example, the luminosity of a $5 M_{Jup}$ planet drops by 2 – 3 orders of magnitude in this time span, while its effective temperature decreases from 1300 to 400 K (Baraffe et al. 2003). Also, the fraction of debris disks around AFGK, and possibly M stars, decreases significantly by ~ 150 Myr (Rieke et al. 2005; Hillenbrand et al. 2008).

The value of young low-mass stars is demonstrated by the ≈ 12 Myr-old star AU Mic, the first robustly identified M dwarf debris disk system (Song et al. 2002; Liu et al. 2004). The AU Mic disk has been the subject of intense scrutiny since its discovery. At a distance of only 10 pc, its disk is seen in scattered light as far as $20''$ in radius (Kalas et al. 2004). Adaptive optics and *HST* imaging of the disk achieves a spatial resolution of 0.4 AU (e.g., Liu et al. 2004; Krist et al. 2005; Fitzgerald et al. 2007) and reveals a rich variety of substructure. The proximity and edge-on geometry of the disk allow for very sensitive studies of the circumstellar gas content (Roberge et al. 2006; France et al. 2007) and searches for transiting planets (Hebb et al. 2007). However, thus far this system remains the singular example of a resolved debris disk around a low-mass star. Thus, the scientific potential of young M dwarfs remains largely untapped due to the very limited current census.

2. Sample Selection

The Two Micron All Sky Survey (2MASS) is optimal for finding low-mass stars, since the SEDs of cool stars peak in the near-IR (e.g. Hawley et al. 2002). However, the *JHK* infrared passbands provide less distinctive spectral classification of early- and mid-M dwarfs (i.e. M2–M7 dwarfs have $(J - K)$ colors which span only 0.2 mag; Reid et al. 2007b) impeding the photometric distance determination. Thus, in order to fully characterize a volume-limited sample of young M dwarfs, a proper motion requirement of $\mu > 0.18'' \text{ yr}^{-1}$ was implemented, equivalent to a tangential velocity of 21 km s^{-1} at 25 pc.

We drew ≈ 800 targets from the NStars 20-pc census (Reid et al. 2003, 2004) constructed from the 2MASS catalogs (Skrutskie et al. 2006) along with the Lépine et al. (2002) and

Lépine & Shara (2005) proper motion catalogs. In addition to these, we included ~ 300 newly-catalogued M dwarfs that exhibit significant proper motion between the POSSI and 2MASS surveys (i.e. the Moving-M sample; Reid et al. 2007a). Reid et al. (2003, 2004, 2007a) used a combination of photometric (i.e. $(V - J) \geq 3$ and $(H - K_s) \geq 0.23$ to largely eliminate stars earlier than M0) and proper-motion methods to identify candidate cool objects, which were subsequently confirmed with follow-up moderate-resolution ($R \sim 1800$) optical spectroscopy. Distances are available either from parallaxes or spectrophotometric relations and are limited to 25 pc from the Sun, good to $\lesssim 15\%$ assuming the stars are single and on the main-sequence (e.g., Reid & Cruz 2002; Cruz et al. 2003). Nearly half of the resulting M dwarfs are not present in the Gliese catalog and have no previously-published spectral types.

As stellar activity is a powerful indicator of youth (open clusters show a consistent and relatively rapid decline in activity with age at a given spectral type; Preibisch & Feigelson 2005), we cross-referenced our total sample of 1103 M dwarfs in the immediate solar neighborhood against the ROSAT All-Sky Survey Bright Source Catalog and Faint Source Catalog (Voges et al. 1999, 2000). Our query was limited to a search radius of $25''$ around the 2MASS coordinates, the 2σ positional error determined by Voges et al. (1999). This returned 364 sources.

Of these, 196 (18% of the full sample and with a median offset between the ROSAT and 2MASS coordinates of $9''$) are strong coronal X-ray emitters with fractional luminosities hovering near the “saturation” level $\log(L_X/L_{bol}) \sim -3$ (e.g. Riaz et al. 2006), ranging across all M dwarf subclasses (Figure 1 & 2). Mismatches with other sources would have been easily identified as the fractional X-ray luminosity of normal stars relative to optical magnitudes is always on the order of 0.1 or less, whereas other X-ray sources, such as galaxies and quasars have fractional luminosities of 1 or greater (Stocke et al. 1991; Zickgraf et al. 2003). In Figure 3 we plot the fractional X-ray flux, F_X/F_J as a function of $(I - J)$, where F_X is the empirically calibrated X-ray flux using the count-rate conversion equation of Schmitt et al. (1995), and F_J is the 2MASS J -band flux. Target stars were chosen to have high X-ray emission ($\log(F_X/F_J) > -2.5$) comparable to or greater than the fractional luminosities of Pleiades members (120 Myr, Micela et al. 1998) and β Pic members (12 Myr, Torres et al. 2006). The 650-Myr-old Hyades stars emit two orders of magnitude less X-ray radiation for early-Ms than the younger samples (Stern et al. 1995). Though data at later spectral types are sparse and the X-ray fluxes of the samples plotted in Figure 3 appear to converge, our targets on average are still significantly stronger X-ray emitters than the late-Ms of the Hyades.

3. The Spectra

We acquired high-resolution échelle spectra of 185 low-mass stars² over 4 nights with the High Resolution Échelle Spectrometer (HIRES; Vogt et al. 1994) on the Keck I 10-m telescope and over 6 nights with the Échelle SpectroPolarimetric Device for the Observation of Stars (ESPaDOnS; Donati et al. 2006) on the Canada-France-Hawaii 3.6-m telescope, both located on the summit of Mauna Kea.

The relevant properties of the targets confirmed to not be spectroscopic binaries (SB) are listed in Table 1. Three of these 155 M dwarfs do not have ROSAT detections but were nonetheless included in the sample due to previously identified youth indicators. (See Table 2 for details.)

We used the 0.861" slit with HIRES to give a spectral resolution of $\lambda/\Delta\lambda \approx 58,000$. The upgraded detector consists of a mosaic of three 2048×4096 15- μm pixel CCDs, corresponding to a blue, green and red chip spanning 4900 – 9300 Å. To maximize the throughput near the peak of a M dwarf spectral energy distribution, we used the GG475 filter with the red cross-disperser. The data product of each exposure is a multi-extension FITS file from which we reduce and extract the data from each chip separately.

ESPaDOnS is fiber fed from the Cassegrain to Coudé focus where the fiber image is projected onto a Bowen-Walraven slicer at the spectrograph entrance. With a 2048×4608 -pixel CCD detector, ESPaDOnS' ‘star+sky’ mode records the full spectrum over 40 grating orders covering 3700 to 10400 Å at a spectral resolution of $\lambda/\Delta\lambda \approx 68,000$. The data were reduced using *Libre Esprit*, a fully automated reduction package provided for the instrument and described in detail by Donati et al. (1997, 2007).

Each stellar exposure was bias-subtracted and flat-fielded for pixel-to-pixel sensitivity variations. After optimal extraction, the 1-D spectra were wavelength calibrated with a Th/Ar arc. Finally the spectra were divided by a flat-field response and corrected for the heliocentric velocity. The final spectra were of moderate S/N reaching 20 – 50 per pixel at 7000 Å. Each night, spectra were also taken of an A0V standard star for telluric line correction and an early-, mid-, and/or late-M radial velocity (RV) standard, which are listed in Table 3.

The high resolution of the data provides RV measurements to better than 1 km s⁻¹ in almost all cases, which can be used in conjunction with a star's distance and proper

²We were unable to secure spectra of 11 of the 196 X-ray sources because they were either too far south to be observed from Mauna Kea and/or too faint, even with the Keck I telescope.

motion to measure its three-dimensional space velocity (UVW). This provides a promising way to determine stellar ages by linking stars kinematically to one of the several known YMGs or associations, which span ages between 8 and 300 Myr (e.g. Zuckerman & Song 2004). However, only 11% of our sample has the required distance precision (<10%) from trigonometric parallaxes to unambiguously associate a star with a single YMG. The bulk of our targets have photometric distances (Reid et al. 2002b), which require an iterative analysis similar to the convergence method developed by Torres et al. (2006) to make meaningful conclusions about group membership. This UVW analysis of our ROSAT sample will be presented in a follow-up paper. Though it should be noted that kinematics alone should not be used to identify young M stars, as demonstrated by the lack of ROSAT detections in several of the proposed YMG members by López-Santiago et al. (2006), e.g. HD 233153, HIP 53020, GJ 466, and HIP 51317.

3.1. Culling of the Spectroscopic Binaries

High-resolution spectra are necessary to identify and remove spectroscopic binaries (SBs) from the sample, since tight binaries have enhanced activity which would erroneously suggests youth. To search for single-lined SBs (SB1), we observed two epochs of 65 targets, none of which showed a significant RV variation between visits. This implies that the single-lined binary fraction in our sample is very low, less than 1.5%, and that M dwarf binaries with low mass ratios ($M_2/M_1 \ll 1$) are rare. We had originally planned to observe all targets twice, but when it became clear that the SB1 fraction was so low, it was no longer good use of telescope time to continue multi-epoch observations of the entire list. These 65 targets are identified in the last column of Table 1.

To search for multi-lined binaries, we cross-correlated each order between 7000 and 9000 Å of each stellar spectrum with a RV standard of similar spectral type using IRAF’s³ *fxcor* routine (Fitzpatrick 1993). We excluded the Ca II infrared triplet (IRT)⁴ and regions of strong telluric absorption in the cross-correlation.

We find a low-mass spectroscopic binary fraction, and therefore contamination rate, of 16%. These 30 SBs are composed of 28 SB2s, 1 SB3 and 1 SB4 (Shkolnik et al. 2008), effectively doubling the number of known low-mass SBs and proving that strong X-ray emission

³IRAF (Image Reduction and Analysis Facility) is distributed by the National Optical Astronomy Observatories, which is operated by the Association of Universities for Research in Astronomy, Inc. (AURA) under cooperative agreement with the National Science Foundation.

⁴The target stars exhibit Ca II emission that is not present in the RV standards.

is an extremely efficient way to find multi-lined SBs.⁵ It is possible that up to 4%⁶ of the 90 stars with a single observation are indeed double-lined SBs if the systems were in conjunction at the times of the observation. Combining this with the $\leq 1.5\%$ chance of observing an SB1, there are at most a handful of undiscovered SBs in Table 1.

4. Spectral Types

The spectra of M dwarfs are dominated by the strong TiO molecular bands (Figure 4), particularly diagnostic of the star’s temperature.⁷ Several TiO band indices have been used throughout the literature to determine the spectral types of M dwarfs, most commonly the TiO5 index of Reid et al. (1995). The more recent TiO-7140 index, defined by Wilking et al. (2005), is the ratio of the mean flux in two 50-Å bands: the ‘continuum’ band centered on 7035 Å and the TiO band on 7140 Å. We chose to use this latter index as our primary diagnostic of SpT because both of the TiO-7140 flux bands appear in a single order in all of our CFHT and Keck spectra.

We calibrated the TiO-7140 index for our data sets against previously measured (Reid et al. 1995) and published (*SIMBAD* and references therein; Wenger et al. 2007) spectral types of 136 M dwarfs we had observed, including several RV standards and known members of the β Pic moving group. Both the linear fits to the CFHT and Keck data sets for stars with SpT earlier than M6 derive spectral types which agree to better than 0.2 subclasses (Figure 5). We therefore combined the sets to get an average fit for the entire sample. The linear relationship used to convert the TiO-7140 index to SpT for M0 – M5 stars is:

$$\text{SpT} = (\text{TiO}_{7140} - 1.0911) / 0.1755, \text{ rms} = 0.6 \quad (1)$$

Here, M0 corresponds to SpT=0, M1 \rightarrow 1, M2 \rightarrow 2, etc. We used this calibration to determine the SpT of the 78 stars in our ROSAT sample which had no previously published spectral types, as well as refine the published values of the others.

We determine the errors of our measurements for the TiO index (and subsequent indices discussed below) by taking the average difference in values determined for the same stars

⁵These details pertaining to these SBs, i.e., orbital velocities, $v\sin i$ ’s, mass ratios, etc., will be published in an upcoming paper.

⁶This 4% limit is based on the time a close-in binary would spend near conjunction such that the RVs of the two components would not produce a resolved cross-correlation function.

⁷See Section 5.1.1 for a discussion on metallicity effects.

observed on different nights. We have 25 Keck targets⁸ and 21 CFHT targets with repeat observations. The measurement errors of the TiO index are larger for the Keck data than for the CFHT data: 0.061 and 0.015, corresponding to 0.33 and 0.11 M subclasses using Eq. 1, respectively. The bulk of the discrepancy in these two errors is attributed to the fiber feed of ESPaDOnS, which illuminates the spectrograph slit uniformly and is thus less affected by variable seeing. Most of the data collected at Keck on 11 May 2006 are particularly plagued by poor seeing, degrading the spectrophotometry used in measuring the indices. If no repeat observation was made, we defer to the published SpT for this run. Although the errors of the TiO index are relatively small, the calibration is based on a sample with SpTs binned to half a subclass, imposing a 0.5 subclass uncertainty in the calculated SpTs listed in Table 1.

For stars of spectral type M6 or later, the TiO band begins to weaken due to saturation and condensation onto grains (Jones & Tsuji 1998) and additional absorption features which depress the “continuum” reference bandpass of the index. Similarly, the VO band at 7300 Å becomes stronger with spectral type and then weakens, but not until after M7, allowing us to unambiguously classify late-type M dwarfs at least until M7. Therefore, for the 17 targets in the sample that are M6 or later, we derived spectral types from visual classification by comparison of the TiO and VO bands with standard stars of known spectral types (Reid et al. 2002a,b, 2003). Again, due to the half-a-subclass binning of published spectral types, the error in the derived SpTs for these late Ms is also ~ 0.5 subclasses.

5. Age-Dating the Sample

X-ray emission is ubiquitous amongst low-mass stars and is indicative of active stellar coronae throughout their lifetimes (e.g. 94% of all K and M dwarfs within 6 pc exhibited detectable X-ray emission as observed by ROSAT; Schmitt et al. 1995). Fractional X-ray luminosities have also been shown to be “saturated” across a wide range of spectral types, H α equivalent widths, and ages at the value of $\log(L_X/L_{\text{bol}}) \sim -3$, with the bulk of the dispersion in both field and cluster samples between $\log(L_X/L_{\text{bol}})$ of -2 and -4 due to variations in stellar rotation (Stauffer et al. 1997; Delfosse et al. 1998).⁹ As shown in Figures 2 and 3, we have selected our sample of M dwarfs with high fractional X-ray luminosities as compared with

⁸Though we have an additional 19 Keck targets with repeat observations, the seeing on one of the two nights was too poor to measure the TiO and CaH indices.

⁹It has been well-established that the chromospheric activity and coronal emission of FGKM stars steadily decreases with age due to the reduced dynamo production of magnetic fields as the star spins down. Unlike the spin-down time-scale for higher-mass stars (<1 Gyr; e.g. Skumanich 1972), the spin-down time-scales for field M dwarfs range from 1 to 10 Gyr, taking longer with decreasing stellar mass (Delfosse et al. 1998).

the Pleiades, all near the X-ray saturation level. And though data at later spectral types are sparse, our targets do not have X-ray fluxes as low as Hyades members.

X-ray emission of M dwarfs declines almost linearly in log-log space from ~ 1 Myr to the about 650 Myr, the age of the Hyades, with a more rapid drop off after that (Preibisch & Feigelson 2005). Using the Preibisch & Feigelson (2005) relation of $L_X \sim t^{-0.75}$ for X-ray luminosity decline, we determine that the bulk of our objects are less than 280 Myr old. We thus estimate an age of $\lesssim 300$ Myr for our sample of 144 targets, with the early Ms ($I - J < 1.2$, SpT $< M2.5$), which have F_X/F_J well above Hyades members, likely less than 150 Myr. This proportion of young stars (144 of 1103) is roughly consistent with expected number of young stars found in the Galactic disk assuming a uniform star-formation history.

We cannot however use X-ray activity to refine the stellar ages beyond this point, as the 150 Myr and 300 Myr limits discussed above are statistical in nature rather than applicable to individual stars.”. Additional age diagnostics are necessary to better characterize and date individual stars. The spectroscopic age indicators available to us such as surface gravity, lithium absorption, and H α emission are discussed below, each with its implications and limitations.

5.1. Surface Gravity

A pre-main-sequence (PMS) star exhibits lower surface gravity as it has not yet fully contracted onto the main-sequence (MS). Even without measuring accurate values for surface gravities, the relative metric of a gravity index provides upper limits on the age of a low-g star using PMS stellar evolution models. Such models show that lower-mass stars take longer to contract to the MS, e.g. a $0.5 M_\odot$ star (SpT $\approx M1$) will reach the main sequence within 100 Myr whereas a $0.1 M_\odot$ star (SpT $\approx M8.5$) will do so in 1 Gyr (D’Antona & Mazzitelli 1994).

The prominent CaH molecular absorption bands (Figure 4) in M dwarf optical spectra are often used as gravity indicators. Typically, M dwarf spectra are collected with lower resolution due to their intrinsic faintness and as such require broad 30–50Å-wide indices. We measured two indices defined in the literature: (1) “Ratio A” from Kirkpatrick et al. (1991), which is defined as the ratio of the mean intensity in two passbands, a “continuum” band and a molecular absorption band of CaH $\lambda 6975$: $[7020-7050\text{\AA}]/[6960-6990\text{\AA}]$, and (2) the “CaH3” ratio from Reid et al. (1995), $[6960-6990\text{\AA}]/[7042-7046\text{\AA}]$. Figure 6 shows how the two indices are strongly correlated. We focus the rest of our discussion using the first index for which the relative errors in our sample are slightly smaller. Since we have 15–20

times the resolution of previous M dwarf surveys, we also defined a narrower 5-Å CaH index $[7044\text{--}7049]/[6972.5\text{--}6977.5]$ providing a more discriminating scale with which to identify low-gravity stars. Both indices are plotted as function of SpT in Figure 7.

5.1.1. The effects of higher metallicity

An important caveat to using the TiO and CaH molecules as temperature and gravity diagnostics is their dependence on metallicity. Higher metallicity will mimic later spectral types and lower surface gravities. Woolf & Wallerstein (2006) demonstrate this metallicity dependence for M dwarfs using the TiO5 and CaH2 indices defined in Reid et al. (1995). Though the data are quite limited, we can estimate from Figure 4 of Woolf & Wallerstein (2006) that in order to increase the calculated SpT by 0.5 subclasses or decrease the CaH-wide index by 0.1, an M dwarf would need to have a $[\text{Fe}/\text{H}]$ enhancement of ≈ 0.5 dex relative to the population’s mean metallicity. Unfortunately, measuring metallicities directly from atomic lines in M dwarf spectra remains difficult and calibration errors usually range from 0.2–0.3 dex and are likely higher (e.g. Bonfils et al. 2005; Woolf & Wallerstein 2006; Bean et al. 2006). However, using the age-metallicity relation for FGK stars in the local Galactic disk as measured by Reid et al. (2007b) and assuming the same metallicity distribution for nearby Ms as for higher mass stars, our young targets should have a mean $[\text{Fe}/\text{H}]$ of 0.11 with a dispersion of 0.18 dex, implying that very few, if any, of our targets will have high enough metallicities to falsely appear as low-g stars in Figure 7.

This metallicity effect is, however, apparent in the placement of the RV standards in the CaH-SpT distribution. They are near or below the locus of the β Pic members and would therefore be flagged as low-g, when they should, in general, be old field stars. None of the standards appears to have low-g from its EW_{KI} and only 5 of 10 have ROSAT detections, all lying well below the target sample in Figure 3. The RV standards exhibit no other evidence of youth, less LHS 2065 and GJ 406, which are both known to be flare stars (Schmitt & Liefke 2002; Schmitt et al. 2008). We attribute their apparent low surface gravity to our choice of the most stable RV standards from Nidever et al. (2002) and Marcy & Benitz (1989), likely due to their stronger absorption lines from higher metallicity. Published $[\text{Fe}/\text{H}]$ values based on the Bonfils et al. (2005) calibration range from -0.16 to $+0.15$ (see Table 3), and do not agree with this conclusion. However, recently Johnson & Apps (2009) pointed out errors in the Bonfils calibration that underestimates M dwarf metallicities by 0.32 dex on average. Using the revised photometric calibration of Johnson & Apps, it is clear from Figure 8 that the bulk of our RV standards are indeed metal rich.

It is clear now that for a sample of field stars with no metallicity measurements, a single

gravity index may not be sufficient. The atomic alkali lines of K I (λ 7665 and 7699Å) and Na I (λ 8183 and 8195Å) may also be used as gravity indicators (e.g. Slesnick et al. 2006). Yet, care is required with these lines as well as they are affected by stellar activity such that higher levels of chromospheric emission fill in the absorption cores and reduce the measured EWs. We settled on the K I line as this filling-in is stronger in the Na I (Reid & Hawley 1999).

Combining the effects of the chromosphere on K I with the uncertainties in metallicity on the TiO and CaH indices, we consider a target as having low-g only if both the CaH and K I measurements indicate that it is so. We flag a target as such in Table 2 if it falls on or below (within error bars) the best-fit curves to the observed β Pic members in Figures 7 and 10. The equations for these curves are listed in the figure captions.

Though we do not have spectra of known young stars at SpTs later than M6.5 with which to calibrate the CaH indices, extrapolating the β Pic curve might imply that all the late Ms in our sample lie in the low-g regime of Figure 7. This is reassuring since PMS evolutionary models (e.g. D’Antona & Mazzitelli 1994) predict a M6.5 ($0.15 M_{\odot}$) star will reach the main-sequence in 500 Myr. Therefore, we would expect that for a sample of X-ray-selected targets with ages $\lesssim 300$ Myr, all late Ms will have low surface gravities.¹⁰

5.2. Lithium detection

PMS stars across all M subclasses are not hot enough to destroy their primordial Li abundance ($T > 2.5 \times 10^6$ K) and are easily identified by their strong lithium absorption at 6708 Å ($EW_{Li} > 0.6$ Å).¹¹ Very young late-K and early-M dwarfs deplete their lithium by a factor of 2 in less than 10 Myr, providing a robust way to discriminate between 8-Myr old stars, such as TWA or η Cha members, and 12-Myr old β Pic members. This depletion is substantially slowed in lower mass stars, such that by M6 a lithium detection sets a 90-Myr upper limit on the star’s age (Chabrier et al. 1996; Stauffer et al. 1998).

¹⁰ Alternative models by Burrows et al. (1993) predict that the radius, and thus the gravity, of a $0.15 M_{\odot}$ star will reach its final size in 250 Myrs.

¹¹ Kirkpatrick et al. (2008) recently pointed out that both theory and observations (albeit weakly) suggest a weakened Li absorption at very young ages of very-late-M and L dwarfs due to their extremely low gravity. As the pre-MS star contracts, it reaches a maximum observed Li strength at about 100 Myr before it begins to weaken again due to Li burning.

We have measured lithium EWs¹² in 8 of our targets, listed in Table 5 and plotted in Figure 11. The lithium in the two earliest of these, GJ 9809 (M0.3) and GJ 3305 (M1.1) sets a limit on their ages of 20–30 Myr, consistent with their known membership of the AB Dor (López-Santiago et al. 2006) and β Pic (Torres et al. 2006) YMGs, respectively. The spectra of the four strongest lithium absorbers 2MASS J1553 (M3.5), 2MASS J2234 (M6), 2MASS J0557 (M7), and 2MASS J0335 (M8.5), are shown in Figures 12.¹³ According to stellar evolution models by Chabrier et al. (1996), a M3.5 star such as 2MASS J1553 with lithium absorption must be less than 40 Myr old. For the ages of other stars, the models can only place upper limits between 90 and 150 Myr. However, 3 of these 4 stars (2MASS J1553, 2MASS J2234, and 2MASS J0335) have $EW_{Li} > 0.6 \text{ \AA}$, implying that they are PMS stars and must be younger than 10 Myr (Zuckerman & Song 2004), consistent with their accretion-level H α emission discussed in the following section.

5.3. H α from accretion

Accretion by PMS stars produces a strong emission-line spectrum, which in the visible includes the Balmer series, caused by accreting gas falling along magnetic field lines from the circumstellar disk onto the star. The near free-fall velocities result in accretion shocks producing both strong and extremely velocity-broadened (\sim hundreds of km s^{-1}) H α emission profiles. The equivalent width and/or velocity width of H α is often used as an indicator of accretion and can set a very young upper limit of 10 Myr on the age of a given star (e.g. Barrado y Navascués & Martín 2003).

We measured the H α EWs of all targets and plot them in Figure 13 as a function of SpT. Eleven of the targets have no significant emission (i.e. $> -1 \text{ \AA}$) and none has H α in absorption. The bright X-ray emission detected by ROSAT from these chromospherically *inactive* stars was likely then the result of a stellar flare, rather than enhanced activity due to youth. The remaining 93% of the ROSAT-selected objects show H α in emission with a clear trend towards higher emission with later spectral type. This is in general attributed to the “contrast effect” as the photospheric luminosity decreases in the *R*-band with lower

¹²The lithium abundances have not been corrected for possible contamination with the Fe I line at 6707.44 \AA . Uncertainties in the setting of continuum levels prior to measurement induce EW errors of about 10–20 m \AA with a dependence on the S/N in the region. We therefore consider our 2σ detection limit to be 0.05 \AA .

¹³2MASS J1553 appeared as a visual binary with the acquisition camera on Keck I and the observations presented in this paper are of the southern component. Allers et al. (in press) have observed 2MASS J2234 as a 0.16” binary with Keck’s laser guide star adaptive optics system, but as we were unable to resolve the system, our spectra are a composite of the two.

effective temperatures (Basri & Marcy 1995). However, comparisons within a narrow range of spectral types can be made to identify more chromospherically active and potentially accreting young objects.

Eight stars in Figure 13 have $\text{H}\alpha$ emission near the empirical accretion/non-accretion boundary (Barrado y Navascués & Martín 2003) depicted by the dashed curve in the figure. Though the accretion curve is not thought to be very robust for objects of SpT later than M5.5, due to the few late-M cluster members used to calibrate the sequence, it does serve as an outer envelope of the chromospheric emission. Unfortunately, this “saturation” criterion is not robust enough to be used exclusively. This is demonstrated by the flaring stars 1RXS J0414, GJ 316.1 and LHS 2065 (Schmitt 1994; Schmitt & Liefke 2002). Though they are likely much younger than 300 Myr, none is accreting, as indicated by the lack of lithium in their spectra.

The empirical “10%-width” metric, which measures the full width at the 10% level of the $\text{H}\alpha$ velocity profile peak, is a more promising diagnostic of accretion. White & Basri (2003) use a combination of $\text{EW}_{\text{H}\alpha} < -10 \text{ \AA}$ and a velocity width of $>200 \text{ km/s}$ to identify accreting T Tauri stars. Mohanty et al. (2005) use $\text{He I } \lambda 6678$ emission as yet another accretion indicator, though several of the objects they determined to be accreting do not exhibit He I emission, while others with He I emission show no signs of accretion. This appears to be the case in our sample as well. Seventeen of our targets have detectable He I emission though the bulk of them are certainly not accretors.

2MASS J2234, 2MASS J1553, 2MASS J0557, and 2MASS J0335 all have lithium absorption, indications of low- g from both the CaH *and* K I diagnostics, and broad $\text{H}\alpha$ profiles, plotted in Figure 14 with average 10%-widths of 306, 446, 207, and 273 km s^{-1} , respectively. Only two however exhibit He I emission. (See Table 5.) Though 2MASS J0335 does not have a strong enough $\text{EW}_{\text{H}\alpha}$ to exceed the Barrado y Navascués & Martín (2003) accretion limit, its $\text{EW}_{\text{H}\alpha}$ of -10.7 \AA does qualify it as an accretor using the White & Basri (2003) criteria. We conclude that 2MASS J2234, 2MASS J1553 and 2MASS J0335 are accreting T Tauri stars while 2MASS J0557 is on the borderline, with upper limits on the ages of 5, 3, 10, and 10 Myr, respectively, based on the criteria devised by White & Basri (2003), Mohanty et al. (2005), and Barrado y Navascués & Martín (2003). Using gravity-sensitive spectral features in the near-IR, Allers et al. (in press) further refined the age of 2MASS J2234 to a very young ~ 1 Myr.

6. Summary

We present our ground-based spectroscopic survey of 185 X-ray-bright low-mass stars, most of which are within 25 pc. Our high-resolution optical spectra allowed us to identify 30 SBs which are strong X-ray emitters, but not necessarily young. For the remainder of the sample, we measured youth indicators such as wide- and narrow-band gravity indices of the CaH molecular band as well as K I equivalent widths. We find that for a sample of field stars with no metallicity measurements, a single gravity index may not be sufficient, as high metallicities mimic low- g on a CaH-SpT plot. This is apparent in a metal-rich sub-sample of our RV standards, which appear to have low surface gravity as measured by the CaH index, yet show no other evidence of youth. Combining the effects of chromospheric activity on EW_{KI} with the uncertainties in metallicity on the TiO and CaH indices, we require that both the CaH *and* K I measurements indicate low- g before classifying a star as such. We have also detected lithium absorption, a sure sign of youth, in 8 targets, 4 of which show evidence of accretion from their velocity-broadened $\text{H}\alpha$ profiles.

We estimate that our final sample of the 144 youngest and nearest low-mass objects in the field is less than \sim 300 Myr old, with 30% of them being younger than 150 Myr old and 4 very young (\lesssim 10 Myr old). This sample provides a rich set of well-characterized targets with the primary requirements of youth and proximity for intensive disk evolution and planet formation studies with ground-based (e.g. adaptive optics) and space-based observations. Two such programs are currently underway: (1) We are using the Multiband Imaging Photometer for the Spitzer Space Telescope (MIPS) to extend debris disk studies to low-mass stars with sufficient sensitivity for meaningful comparison with higher mass stars. Also, the newly discovered disks will be among the closest to Earth, making them prime targets for multiwavelength and high angular resolution followup. (2) The Gemini Planet-Finding Campaign (Liu et al. 2009), an extensive (500 hours) search for massive extrasolar planets using the high-contrast AO Near-Infrared Coronagraphic Imager (NICI), has observed many of our targets and will continue to do so over the next two years. This program will provide key constraints for the separation distributions of extrasolar planets at 5 – 10 AU, the dependence on planet frequency on stellar host mass, and the spectral properties of extrasolar giant planets.

E.S thanks the CFHT and Keck staff for their care in setting up the instruments and support in the control rooms, and to Jean-Francois Donati for making Libre-ESpRIT available to CFHT. E.S. also thanks John Johnson for useful discussions and stepping in to observe one night, and the anonymous referee for a detailed and helpful review of the manuscript. Research funding from the NASA Postdoctoral Program (formerly the NRC Research Associate

ateship) and the Carnegie Institution of Washington for E.S. is gratefully acknowledged. This material is also based upon work supported by the National Aeronautics and Space Administration through the NASA Astrobiology Institute and the NASA/GALEX grant program under Cooperative Agreement Nos. NNA04CC08A and NNX07AJ43G issued through the Office of Space Science. M.C.L. acknowledges support from the Alfred P. Sloan Research Fellowship. This publication makes use of data products from the Two Micron All Sky Survey, which is a joint project of the University of Massachusetts and the Infrared Processing and Analysis Center/California Institute of Technology, funded by the National Aeronautics and Space Administration and the National Science Foundation.

REFERENCES

Allen, P. R., & Reid, I. N. 2008, AJ, 135, 2024

Baraffe, I., Chabrier, G., Barman, T. S., Allard, F., & Hauschildt, P. H. 2003, A&A, 402, 701

Barrado y Navascués, D., & Martín, E. L. 2003, AJ, 126, 2997

Basri, G., & Marcy, G. W. 1995, AJ, 109, 762

Bean, J. L., Sneden, C., Hauschildt, P. H., Johns-Krull, C. M., & Benedict, G. F. 2006, ApJ, 652, 1604

Beuzit, J.-L., et al. 2004, A&A, 425, 997

Bochanski, J. J., Hawley, S. L., Reid, I. N., Covey, K. R., West, A. A., Golimowski, D. A., & Ivezić, Z. 2008, ArXiv e-prints

Bonfils, X., Delfosse, X., Udry, S., Santos, N. C., Forveille, T., & Ségransan, D. 2005, A&A, 442, 635

Burrows, A., Hubbard, W. B., Saumon, D., & Lunine, J. I. 1993, ApJ, 406, 158

Casagrande, L., Flynn, C., & Bessell, M. 2008, MNRAS, 389, 585

Chabrier, G., Baraffe, I., & Plez, B. 1996, ApJ, 459, L91+

Covey, K. R., et al. 2008, ApJS, 178, 339

Cruz, K. L., et al. 2007, AJ, 133, 439

Cruz, K. L., Reid, I. N., Liebert, J., Kirkpatrick, J. D., & Lowrance, P. J. 2003, AJ, 126, 2421

Daemgen, S., Siegler, N., Reid, I. N., & Close, L. M. 2007, ApJ, 654, 558

D'Antona, F., & Mazzitelli, I. 1994, ApJS, 90, 467

Delfosse, X., Forveille, T., Perrier, C., & Mayor, M. 1998, A&A, 331, 581

Donati, J.-F., Catala, C., Landstreet, J. D., & Petit, P. 2006, in Astronomical Society of the Pacific Conference Series, Vol. 358, Astronomical Society of the Pacific Conference Series, ed. R. Casini & B. W. Lites, 362–+

Donati, J.-F., et al. 2007, MNRAS, 380, 1297

Donati, J.-F., Semel, M., Carter, B. D., Rees, D. E., & Collier Cameron, A. 1997, MNRAS, 291, 658

Fitzgerald, M. P., Kalas, P. G., Duchêne, G., Pinte, C., & Graham, J. R. 2007, ApJ, 670, 536

Fitzpatrick, M. J. 1993, in Astronomical Society of the Pacific Conference Series, Vol. 52, Astronomical Data Analysis Software and Systems II, ed. R. J. Hanisch, R. J. V. Brissenden, & J. Barnes, 472–+

France, K., Roberge, A., Lupu, R. E., Redfield, S., & Feldman, P. D. 2007, ApJ, 668, 1174

Gershberg, R. E., Katsova, M. M., Lovkaya, M. N., Terebikh, A. V., & Shakhovskaya, N. I. 1999, A&AS, 139, 555

Hawley, S. L., et al. 2002, AJ, 123, 3409

Hebb, L., Petro, L., Ford, H. C., Ardila, D. R., Toledo, I., Minniti, D., Golimowski, D. A., & Clampin, M. 2007, MNRAS, 379, 63

Hillenbrand, L. A., et al. 2008, ApJ, 677, 630

Hünsch, M., Schmitt, J. H. M. M., Sterzik, M. F., & Voges, W. 1999, A&AS, 135, 319

Ida, S., & Lin, D. N. C. 2008, ApJ, 673, 487

Jeffries, R. D. 1995, MNRAS, 273, 559

Johnson, J. A., & Apps, K. 2009, ArXiv e-prints

Jones, H. R. A., & Tsuji, T. 1998, in Astronomical Society of the Pacific Conference Series, Vol. 134, Brown Dwarfs and Extrasolar Planets, ed. R. Rebolo, E. L. Martin, & M. R. Zapatero Osorio, 423–+

Kalas, P., Liu, M. C., & Matthews, B. C. 2004, Science, 303, 1990

Kirkpatrick, J. D., et al. 2008, ApJ, 689, 1295

Kirkpatrick, J. D., Henry, T. J., & McCarthy, Jr., D. W. 1991, ApJS, 77, 417

Krist, J. E., et al. 2005, AJ, 129, 1008

Lépine, S., & Shara, M. M. 2005, AJ, 129, 1483

Lépine, S., Shara, M. M., & Rich, R. M. 2002, AJ, 124, 1190

Li, J. Z., & Hu, J. Y. 1998, A&AS, 132, 173

Liu, M. C., Matthews, B. C., Williams, J. P., & Kalas, P. G. 2004, ApJ, 608, 526

Liu, M. C., et al. 2009, in American Institute of Physics Conference Series, Vol. 1094, American Institute of Physics Conference Series, ed. E. Stempels, 461–464

López-Santiago, J., Montes, D., Crespo-Chacón, I., & Fernández-Figueroa, M. J. 2006, ApJ, 643, 1160

Lyo, A.-R., Lawson, W. A., & Bessell, M. S. 2004, MNRAS, 355, 363

Mandell, A. M., Raymond, S. N., & Sigurdsson, S. 2007, ApJ, 660, 823

Marcy, G. W., & Benitz, K. J. 1989, ApJ, 344, 441

McCarthy, C., Zuckerman, B., & Becklin, E. E. 2001, AJ, 121, 3259

Micela, G., Sciortino, S., Harnden, Jr., F. R., & Rosner, R. 1998, Ap&SS, 261, 105

Mohanty, S., Jayawardhana, R., & Basri, G. 2005, ApJ, 626, 498

Montes, D., López-Santiago, J., Fernández-Figueroa, M. J., & Gálvez, M. C. 2001, A&A, 379, 976

Nidever, D. L., Marcy, G. W., Butler, R. P., Fischer, D. A., & Vogt, S. S. 2002, ApJS, 141, 503

Norton, A. J., et al. 2007, A&A, 467, 785

Perryman, M. A. C., & ESA, eds. 1997, ESA Special Publication, Vol. 1200, The HIPPARCOS and TYCHO catalogues. Astrometric and photometric star catalogues derived from the ESA HIPPARCOS Space Astrometry Mission

Pettersen, B. R. 1980, PASP, 92, 188

Preibisch, T., & Feigelson, E. D. 2005, ApJS, 160, 390

Reid, I. N., & Cruz, K. L. 2002, AJ, 123, 2806

Reid, I. N., et al. 2003, AJ, 126, 3007

—. 2004, AJ, 128, 463

Reid, I. N., Cruz, K. L., & Allen, P. R. 2007a, AJ, 133, 2825

Reid, I. N., Gizis, J. E., & Hawley, S. L. 2002a, AJ, 124, 2721

Reid, I. N., & Hawley, S. L. 1999, AJ, 117, 343

Reid, I. N., Hawley, S. L., & Gizis, J. E. 1995, AJ, 110, 1838

Reid, I. N., Kirkpatrick, J. D., Liebert, J., Gizis, J. E., Dahn, C. C., & Monet, D. G. 2002b, AJ, 124, 519

Reid, I. N., Turner, E. L., Turnbull, M. C., Mountain, M., & Valenti, J. A. 2007b, ApJ, 665, 767

Reid, I. N., & Walkowicz, L. M. 2006, PASP, 118, 671

Riaz, B., Gizis, J. E., & Harvin, J. 2006, AJ, 132, 866

Rieke, G. H., et al. 2005, ApJ, 620, 1010

Roberge, A., Feldman, P. D., Weinberger, A. J., Deleuil, M., & Bouret, J.-C. 2006, Nature, 441, 724

Schmitt, J. H. M. M. 1994, ApJS, 90, 735

Schmitt, J. H. M. M., Fleming, T. A., & Giampapa, M. S. 1995, ApJ, 450, 392

Schmitt, J. H. M. M., & Liefke, C. 2002, A&A, 382, L9

Schmitt, J. H. M. M., Reale, F., Liefke, C., Wolter, U., Fuhrmeister, B., Reiners, A., & Peres, G. 2008, A&A, 481, 799

Shkolnik, E., Liu, M. C., Reid, I. N., Hebb, L., Cameron, A. C., Torres, C. A., & Wilson, D. M. 2008, ApJ, 682, 1248

Skrutskie, M. F., et al. 2006, AJ, 131, 1163

Skumanich, A. 1972, ApJ, 171, 565

Slesnick, C. L., Carpenter, J. M., & Hillenbrand, L. A. 2006, AJ, 131, 3016

Song, I., Weinberger, A. J., Becklin, E. E., Zuckerman, B., & Chen, C. 2002, AJ, 124, 514

Stauffer, J., Klemola, A., Prosser, C., & Probst, R. 1991, AJ, 101, 980

Stauffer, J. R., Balachandran, S. C., Krishnamurthi, A., Pinsonneault, M., Terndrup, D. M., & Stern, R. A. 1997, *ApJ*, 475, 604

Stauffer, J. R., Schultz, G., & Kirkpatrick, J. D. 1998, *ApJ*, 499, L199+

Stern, R. A., Schmitt, J. H. M. M., & Kahabka, P. T. 1995, *ApJ*, 448, 683

Stocke, J. T., Morris, S. L., Gioia, I. M., Maccacaro, T., Schild, R., Wolter, A., Fleming, T. A., & Henry, J. P. 1991, *ApJS*, 76, 813

Torres, C. A. O., Quast, G. R., da Silva, L., de La Reza, R., Melo, C. H. F., & Sterzik, M. 2006, *A&A*, 460, 695

Torres, C. A. O., Quast, G. R., Melo, C. H. F., & Sterzik, M. F. 2008, Young Nearby Loose Associations (Handbook of Star Forming Regions, Volume II: The Southern Sky ASP Monograph Publications, Vol. 5. Edited by Bo Reipurth, p.757), 757–+

Voges, W., et al. 1999, *A&A*, 349, 389

—. 2000, VizieR Online Data Catalog, 9029, 0

Vogt, S. S., et al. 1994, in Society of Photo-Optical Instrumentation Engineers (SPIE) Conference Series, Vol. 2198, Society of Photo-Optical Instrumentation Engineers (SPIE) Conference Series, ed. D. L. Crawford & E. R. Craine, 362–+

Webb, R. A., Zuckerman, B., Platais, I., Patience, J., White, R. J., Schwartz, M. J., & McCarthy, C. 1999, *ApJ*, 512, L63

Wenger, M., et al. 2007, in Astronomical Society of the Pacific Conference Series, Vol. 377, Library and Information Services in Astronomy V, ed. S. Ricketts, C. Birdie, & E. Isaksson, 197–+

West, A. A., Hawley, S. L., Bochanski, J. J., Covey, K. R., Reid, I. N., Dhital, S., Hilton, E. J., & Masuda, M. 2008, *AJ*, 135, 785

White, R. J., & Basri, G. 2003, *ApJ*, 582, 1109

Wilking, B. A., Meyer, M. R., Robinson, J. G., & Greene, T. P. 2005, *AJ*, 130, 1733

Woolf, V. M., & Wallerstein, G. 2005, *MNRAS*, 356, 963

—. 2006, *PASP*, 118, 218

Zickgraf, F.-J., Engels, D., Hagen, H.-J., Reimers, D., & Voges, W. 2003, *A&A*, 406, 535

Zickgraf, F.-J., Krautter, J., Reffert, S., Alcalá, J. M., Mujica, R., Covino, E., & Sterzik, M. F. 2005, *A&A*, 433, 151

Zuckerman, B., & Song, I. 2004, *ARA&A*, 42, 685

Zuckerman, B., Song, I., & Bessell, M. S. 2004, *ApJ*, 613, L65

Table 1. Observed M dwarfs

Name ^a	RA & DEC J2000 (2MASS)	Tele- scope ^b	SpT M-(±0.5) ^b	Dist. ^c (pc)	<i>I</i> <i>USNO</i>	<i>J</i> <i>2MASS</i>	$\log(F_X/F_J)^d$	Binarity ⁱ
2MASS J00034227-2822410	00 03 42.28 -28 22 41.0	Keck	7.0 ^e	29.2±4.0	15.65	13.068	-1.742	--
G 217-32	00 07 42.64 60 22 54.3	CFHT	3.8	12.2±1.7	10.32	8.911	-2.391	--
LP 348-40	00 11 53.03 22 59 04.8	CFHT	3.5	16.0±2.7	10.22	8.862	-1.824	SB+
NLTT 614	00 12 57.17 50 59 17.3	Keck	6.4	18.2±2.7	13.65	11.406	-2.041	--
1RXS J001557.5-163659	00 15 58.08 -16 36 57.9 ^j	CFHT	4.1	7.3±1.2	10.49	8.736	-2.430	SB+
GJ 1006 A	00 16 14.56 19 51 38.6	Keck	3.6	12.3±2.7	—	7.875	-2.446	$P_{phot}=4.7901$ d (Norton et al. 2007) ^f
GJ 3030	00 21 57.81 49 12 38.0	CFHT	2.4	24.1±2.7	10.12	9.139	-2.610	--
GJ 3036	00 28 53.92 50 22 33.0	CFHT	3.7	17.4±4.5	10.28	8.847	-2.222	0.426" VB (Daemgen et al. 2007)
NLTT 1875	00 35 4.88 59 53 08.0	Keck	4.3	19.5±2.7	12.58	11.039	-2.173	--
G 69-32	00 54 48.03 27 31 03.6 ^j	Keck	4.6	17.8±4.5	11.59	10.34	-2.179	--
G 132-51B (W)	01 03 42.11 40 51 15.8 ^j	CFHT	2.6	29.3±2.7	10.32	9.372	-1.729	VB (brighter) (this work), SB+
G 132-51B (E)	01 03 42.11 40 51 15.8	CFHT	3.8	29.3±2.7	10.32	9.372	-1.729	VB (fainter) (this work)
G 269-153 (NE)	01 24 27.68 -33 55 08.6 ^j	CFHT	4.3	12.6±2.3	10.47	9.203	-2.096	2.065" VB (Daemgen et al. 2007), SB+
G 269-153 (SW)	01 24 27.68 -33 55 08.6	CFHT	4.6	12.6±2.3	10.47	9.203	-2.096	2.065" VB (Daemgen et al. 2007), SB+
G 172-56	01 29 12.57 48 19 35.5	Keck	5.4	44.0±7.4	12.07	10.912	-1.809	--
2MASS J01351393-0712517	01 35 13.93 -07 12 51.8 ^j	CFHT	4.3	9.0±1.5	10.46	8.964	-2.304	--
G 271-110	01 36 55.17 -06 47 37.9	CFHT	3.5	25.8±4.2	11.02	9.707	-2.125	SB+
LHS 6032 (SW)	01 45 18.2 46 32 07.8	CFHT	1.3	26.7±2.7	9.94	8.058	-2.130	VB (this work)
1RXS J015027.1-185134	01 50 27.12 -18 51 36.0	Keck	5.4	—	13.31	11.484	-1.985	--
NLTT 6549	01 58 13.61 48 44 19.7	CFHT	1.5	23.4±2.7	10.13	9.123	-2.554	--
GJ 1041A (SW)	01 59 12.39 03 31 09.2	CFHT	0.6	22.5±2.7	9.8	7.906	-2.450	--
GJ 82	01 59 23.5 58 31 16.2	CFHT	4.2	9.1±2.7	11.12	7.79	-2.344	--
GJ 3136	02 08 53.6 49 26 56.6	CFHT	2.9	13.7±1.4	9.6	8.423	-2.167	--
1RXS J021836.6+121902	02 18 36.55 12 18 58.0 ^j	CFHT	1.9	20.1±2.7	9.9	8.797	-2.597	--
GJ 3150	02 19 2.29 23 52 55.1	CFHT	3.6	18.4±2.7	10.89	9.777	-2.302	--
1RXS J022735.8+471021	02 27 37.26 47 10 04.5	CFHT	4.6	14.5±2.7	11.47	10.306	-2.418	--
1RXS J023138.7+445640	02 31 39.27 44 56 38.8	CFHT	4.4	12.9±2.4	11.1	9.97	-2.456	--
G 36-26	02 36 44.13 22 40 26.5	CFHT	5.9	12.8±1.1	11.39	10.081	-2.009	--
GJ 3174	02 39 17.35 07 28 17.0	CFHT	3.7	19.7±2.7	11.02	9.881	-2.392	--
LP 247-13	03 15 37.83 37 24 14.3	CFHT	2.7	25.4±4.0	10.49	9.317	-2.204	--
G 246-33	03 19 28.73 61 56 04.6	CFHT	4.1	10.9±2.7	10.92	9.511	-2.169	--
1RXS J032230.7+285852	03 22 31.66 28 58 29.2	Keck	4.0	18.0±2.7	11.89	10.823	-2.119	--
2MASS J03350208+2342356	03 35 2.09 23 42 35.6	Keck	8.5	16.6±2.3	—	12.25	—	--
1RXS J034231.8+121622	03 42 31.8 12 16 22.6 ^j	Keck	5.2	17.9±2.7	11.21	10.157	-2.144	SB+

Table 1—Continued

Name ^a	RA & DEC J2000 (2MASS)	Tele- scope ^b	SpT M-(±0.5) ^b	Dist. ^c (pc)	<i>I</i> <i>USNO</i>	<i>J</i> <i>2MASS</i>	$\log(F_X/F_J)^d$	Binarity ⁱ
G 80-21	03 47 23.33 -01 58 19.5 ^j	Keck	2.8	16.3 ± 0.8	13.02	7.804	-2.346	--
II Tau	03 49 43.25 24 19 04.7	Keck	4.6	20.4 ± 3.8	10.67	9.805	-2.338	--
1RXS J041325.8-013919	04 13 25.76 -01 39 41.7 ^j	Keck	5.3	9.4 ± 1.5	10.94	9.375	-2.312	0.79" VB (McCarthy et al. 2001)
1RXS J041417.0-090650	04 14 17.3 -09 06 54.4 ^j	Keck	4.3	10.6 ± 1.7	11.12	9.63	-1.922	SB+
GJ 3287	04 27 41.3 59 35 16.7	CFHT	3.8	20.1 ± 2.7	11.32	9.975	-2.402	--
GJ 3305	04 37 37.46 -02 29 28.3 ^j	Keck	1.1	15.8 ± 1.6	4.94	7.299	-1.866	--
GJ 3304	04 38 12.56 28 13 00.1	Keck	4.6	14.5 ± 3.8	9.86	8.173	-2.350	0.783" VB (Beuzit et al. 2004; Daemgen et al. 2007)
NLTT 13728	04 40 23.25 -05 30 08.3	Keck	6.0	10.3 ± 0.9	13.08	10.658	-2.139	--
NLTT 13837	04 44 8.15 14 01 22.9	Keck	4.3	28.8 ± 4.4	11.02	9.843	-2.360	--
NLTT 13844	04 45 5.62 43 24 34.2	Keck	4.6	22.5 ± 2.7	13.2	10.84	-2.320	--
2MASS J04465175-1116476	04 46 51.75 -11 16 47.6	Keck	4.9	13.4 ± 2.2	9.56	8.144	-2.486	VB (this work)
2MASS J04472312-2750358	04 47 23.13 -27 50 35.8	Keck	0.5	10.9 ± 1.8	8.43	7.66	-2.148	--
G 81-34	04 49 29.47 48 28 45.9	CFHT	4.0	13.6 ± 2.7	10.55	9.059	-2.379	--
1RXS J045101.0+312734	04 51 1.38 31 27 23.9	Keck	3.7	22.2 ± 2.7	10.25	9.011	-2.209	--
NLTT 14116	04 52 24.41 -16 49 21.9 ^j	Keck	3.3	17.4 ± 1.2	10.43	7.74	-2.389	1.48" G. Anglada-Escudé (priv. com ^b)
GJ 3335	05 09 9.97 15 27 32.5	Keck	3.5	18.3 ± 2.7	10.16	8.77	-2.324	--
NLTT 15049	05 25 41.67 -09 09 12.3 ^j	Keck	3.8	20.2 ± 4.7	10.13	8.454	-2.416	0.537" VB (Daemgen et al. 2007)
GJ 207.1	05 33 44.81 01 56 43.4	Keck	2.0	16.8 ± 1.2^g	10.43	7.764	-2.298	--
1RXS J055446.0+105559	05 54 45.74 10 55 57.1	CFHT	2.1	20.3 ± 2.7	10.23	8.832	-2.337	--
2MASS J05575096-1359503	05 57 50.97 -13 59 50.3	Keck	7.0	26.8 ± 3.7	16.49	12.871	-1.672	--
GJ 3372 B	05 59 55.69 58 34 15.6	CFHT	4.2	12.7 ± 2.7	10.5	9.028	-2.403	--
G 249-36	06 05 29.36 60 49 23.2	CFHT	4.9	10.6 ± 2.7	10.74	9.096	-2.247	--
GJ 3395	06 31 1.16 50 02 48.6	CFHT	0.8	19.6 ± 2.7	9.37	7.873	-2.448	--
G 108-36	06 51 59.02 03 12 55.3	CFHT	2.5	23.4 ± 2.7	10.28	9.139	-2.306	--
GJ 3417 (NE)	06 57 57.04 62 19 19.7	CFHT	5.2	9.5 ± 2.7	10.25	8.585	-2.100	VB (this work)
GJ 2060	07 28 51.38 -30 14 49.1	Keck	1.3	15.8 ± 2.3^g	8.39	6.615	-2.207	VB - quadruple system (Allen & Reid 2008), SB+
GJ 277B	07 31 57.35 36 13 47.8	Keck	3.3	11.5 ± 0.7^g	—	7.571	-2.081	--
1RXS J073829.3+240014	07 38 29.52 24 00 08.8	Keck	2.7	—	10.32	8.928	-2.008	--
NLTT 18549	07 52 23.9 16 12 15.7	Keck	7.0	10.5 ± 0.5	—	10.879	—	SB+
2MASS J07572716+1201273	07 57 27.16 12 01 27.3	Keck	2.3	23.0 ± 3.7	10.03	9.06	-2.411	SB+
2MASS J08031018+2022154	08 03 10.18 20 22 15.5 ^j	Keck	3.3	23.4 ± 3.8	10.34	9.242	-1.899	SB+
GJ 316.1	08 40 29.75 18 24 09.2	Keck	6.0	14.1 ± 0.2	—	11.053	-1.033	SB+
NLTT 20303	08 48 36.45 -13 53 08.4	Keck	2.6	16.4 ± 1.7	9.22	8.748	-1.701	SB+
1RXS J091744.5+461229	09 17 44.73 46 12 24.7	Keck	1.7	18.9 ± 3.0	—	8.126	-2.009	SB+

Table 1—Continued

Name ^a	RA & DEC J2000 (2MASS)	Tele- scope ^b	SpT M-(±0.5) ^b	Dist. ^c (pc)	<i>I</i> <i>USNO</i>	<i>J</i> <i>2MASS</i>	$\log(F_X/F_J)^d$	Binarity ⁱ
G 43-2	09 48 50.2 15 38 44.9	Keck	2.0 ^h	24.3±2.7	—	9.303	-2.419	—
NLTT 22741	09 51 4.6 35 58 09.8	Keck	4.5	23.0±2.7	11.89	10.577	-2.349	M4.5/L6 wide VB (Reid & Walkowicz 2006)
GJ 3577 A (W)	09 59 18.8 43 50 25.6	Keck	3.5 ^e	26.2±2.7	10.72	9.682	-1.922	VB (this work)
G 196-3A	10 04 21.49 50 23 13.6	Keck	3.0 ^e	14.9±2.7	10.74	8.081	-2.063	—
GJ 2079	10 14 19.19 21 04 29.8	Keck	0.7	20.4±0.7 ^g	8.64	7.074	-2.640	—
1RXS J101432.0+060649	10 14 31.95 06 06 41.0	Keck	4.1	17.7±2.7	9.94	8.879	-2.169	VB (< 0.7") (this work)
GJ 388	10 19 36.35 19 52 12.2	Keck	3.5 ^e	4.9±0.1 ^g	7.78	5.449	-2.389	—
G 44-9	10 20 44.07 08 14 23.4	Keck	5.9	20.2±2.7	12.13	10.354	-2.365	—
2MASS J10364483+1521394	10 36 44.84 15 21 39.5	Keck	4.0 ^e	19.6±4.6	10.03	8.748	-2.186	1.061" VB (Daemgen et al. 2007)
GJ 3629	10 51 20.6 36 07 25.6	Keck	3.0 ^e	16.7±2.7	10.63	9.422	-2.187	—
GJ 3639	11 03 10 36 39 08.5	Keck	3.5 ^e	18.6±2.7	10.44	9.464	-2.327	—
NLTT 26114	11 03 21.25 13 37 57.1	Keck	3.0 ^h	14.1±1.5	—	8.759	-2.287	—
G 119-62	11 11 51.76 33 32 11.2	Keck	3.5 ^e	13.6±1.3	9.71	8.297	-2.234	—
1RXS J111300.1+102518	11 13 0.6 10 25 05.9	Keck	3.0 ^h	20.2±2.7	11.39	10.032	-2.201	—
GJ 3653	11 15 54.04 55 19 50.6	Keck	0.5 ^e	22.3±2.7	9.56	8.09	-2.381	—
2MASS J11240434+3808108	11 24 4.35 38 08 10.9	Keck	4.5 ^h	19.2±3.1	10.64	9.928	-2.241	—
G 10-52	11 48 35.49 07 41 40.4	Keck	3.5 ^h	16.0±2.7	10.62	9.476	-2.423	—
2MASS J12065663+7007514 (E)	12 06 56.63 70 07 51.4 ^j	CFHT	4.4	16.8±1.9	9.1	9.251	-1.758	VB (this work)
G 122-74	12 12 11.36 48 49 03.2	Keck	3.5 ^h	23.3±2.7	10.04	9.258	-2.536	VB (this work)
GJ 3729	12 29 2.9 41 43 49.7	Keck	3.5 ^e	15.2±2.7	9.87	8.786	-2.496	—
GJ 3730	12 29 27.13 22 59 46.7	Keck	4.0 ^e	16.7±2.7	11.04	9.823	-2.105	—
1RXS J124147.5+564506	12 41 47.37 56 45 13.8 ^j	Keck	2.5 ^e	26.2±4.2	10.4	9.483	-2.091	—
GJ 490 B	12 57 39.35 35 13 19.5	Keck	4.0 ^e	18.0±1.1 ^g	14.78	8.872	-1.648	—
GJ 490 A	12 57 40.3 35 13 30.6	Keck	0.5 ^e	18.0±1.1 ^g	8.84	7.401	-2.236	$P_{phot}=3.17$ d (Pettersen 1980; Norton et al. 2007) ^f
NLTT 32659 (E)	13 02 5.87 12 22 21.6	Keck	3.7	28.4±2.7	9.96	9.089	-2.337	VB (this work)
NLTT 32659 (W)	13 02 5.87 12 22 21.6	Keck	1.6	28.4±2.7	9.96	9.089	-2.337	VB (this work), SB1
GJ 1167 A	13 09 34.95 28 59 06.6 ^j	Keck	4.8	11.5±2.4 ^g	10.67	9.476	-2.308	SB1
GJ 3786	13 27 19.67 -31 10 39.4 ^j	Keck	3.5 ^e	19.6±4.6	10.89	9.329	-2.327	0.544" VB (Daemgen et al. 2007), SB1
2MASS J13292408-1422122	13 29 24.08 -14 22 12.3 ^j	CFHT	2.8	22.6±3.6	10.42	9.061	-2.531	—
2MASS J14215503-3125537	14 21 55.04 -31 25 53.7	Keck	3.9	—	10.98	9.66	-2.151	SB1
2MASS J1442809-0424078	14 44 28.1 -04 24 07.8 ^j	Keck	3.0	27.5±4.4	11.01	9.728	-2.411	SB1
1RXS J150907.2+590422	15 09 6.96 59 04 28.2 ^j	CFHT	2.2	25.8±4.2	9.66	9.249	-2.356	—
GJ 9520	15 21 52.92 20 58 39.5	Keck	1.0	11.4±0.3	8.41	6.61	-2.485	SB1
NLTT 40561	15 33 50.62 25 10 10.6	Keck	3.5	23.2±2.7	11.31	10.433	-2.282	SB1

Table 1—Continued

Name ^a	RA & DEC J2000 (2MASS)	Tele- scope ^b	SpT M-(±0.5) ^b	Dist. ^c (pc)	<i>I</i> <i>USNO</i>	<i>J</i> <i>2MASS</i>	$\log(F_X/F_J)^d$	Binarity ⁱ
G 167-54	15 43 48.48 25 52 37.7	Keck	4.1	21.1±2.7	11.3	10.022	-2.305	SB+
2MASS J15534211-2049282 (S)	15 53 42.12 -20 49 28.2	Keck	3.4	29.6±2.9	13.44	11.256	—	VB (this work), SB+
GJ 3928	15 55 31.78 35 12 02.9 ^j	CFHT	5.3	12.6±3.6	10.51	8.928	-2.274	1.571" VB (Daemgen et al. 2007)
NLTT 43695 (E)	16 51 9.95 35 55 07.1 ^j	Keck	4.6	34.5±3.9	11.67	10.334	-2.094	VB (this work), SB+
LP 331-57	17 03 52.83 32 11 45.6 ^j	CFHT	2.4	18.0±1.2	10.94	7.886	-2.659	$P_{phot}=15.4221$ d, 1.13" VB (Norton et al. 2007; Daemgen et al. 2007)
GJ 616.2	17 19 52.98 26 30 02.6	Keck	5.6	10.8±0.2 ^g	8.78	8.229	-2.036	SB+
GJ 669A	17 19 54.22 26 30 03.0	Keck	3.4	12.0±0.9 ^g	9.6	7.273	-2.418	SB+
1RXS J173130.9+272134	17 31 29.75 27 21 23.3	Keck	2.6	16.1±2.7	14.94	12.094	-1.507	SB+
G 227-22	18 02 16.6 64 15 44.6 ^j	Keck	6.1	7.1±0.6	9.92	8.541	-2.536	SB+
GJ 4044	18 13 6.57 26 01 51.9	Keck	4.5	12.1±2.7	10.39	8.899	-2.018	VB of LP 390-16, $P_{phot}=2.2838$ d (this work) SB+
LP 390-16	18 13 6.57 26 01 51.9	CFHT	3.8	13.2±1.5	10.39	8.899	-2.018	VB of GJ 4044 (this work)
1RXS J183203.0+203050 (N)	18 32 2.91 20 30 58.1	Keck	4.9	21.6±2.7	11.45	10.653	-1.565	VB (this work), SB+
1RXS J183203.0+203050 (S)	18 32 2.91 20 30 58.1	Keck	5.1	21.6±2.7	11.45	10.653	-1.565	VB (this work), SB+
1RXS J184410.0+712909 (E)	18 44 10.2 71 29 17.6	CFHT	3.9	22.2±2.7	10.73	10.138	-2.502	VB (this work)
1RXS J184410.0+712909 (W)	18 44 10.2 71 29 17.6	CFHT	4.1	22.2±2.7	10.73	10.138	-2.502	VB (this work)
GJ 9652 A	19 14 39.26 19 19 02.6	Keck	4.5	19.1±1.1 ^g	10.46	7.579	-2.335	SB+
2MASS J19303829-1335083	19 30 38.3 -13 35 08.4	Keck	6.0	25.0±4.0	13.61	11.53	-2.269	SB+
1RXS J193124.2-213422	19 31 24.34 -21 34 22.6 ^j	Keck	2.4	19.0±3.1	10.23	8.694	-2.469	SB+
1RXS J193528.9+374605	19 35 29.23 37 46 08.2	Keck	3.0	9.4±2.7	9.91	7.562	-2.514	SB+
1RXS J194213.0-204547	19 42 12.82 -20 45 47.8 ^j	Keck	5.1	10.8±1.7	11.07	9.598	-2.249	SB+
G 125-36	19 50 15.93 31 46 59.9	Keck	2.1	24.2±2.7	10.34	9.178	-2.306	SB+
2MASS J20003177+5921289	20 00 31.77 59 21 29.0	Keck	4.1	20.9±3.4	9.99	9.636	-2.243	SB+
1RXS J204340.6-243410 (NE)	20 43 41.15 -24 33 53.5 ^j	Keck	3.7	24.7±2.8	10.08	8.597	-2.243	VB (this work), SB+
1RXS J204340.6-243410 (SW)	20 43 41.15 -24 33 53.5	Keck	4.1	24.7±2.8	10.08	8.597	-2.243	VB (this work), SB+
NLTT 49856	20 46 43.61 -11 48 13.2 ^j	Keck	4.5	14.6±2.2	10.48	9.349	-2.222	SB+
2MASS J20530910-0133039	20 53 9.1 -01 33 04.0 ^j	CFHT	5.6	16.5±1.5	11.39	10.659	-2.362	SB+
NLTT 50066	20 53 14.65 -02 21 21.9 ^j	CFHT	2.9	23.7±3.8	10.68	9.329	-2.601	—
GJ 4185B	21 16 3.79 29 51 46.0	Keck	3.3	16.1±2.7	10.45	9.295	-1.816	SB+
GJ 4185 A	21 16 5.77 29 51 51.1	Keck	3.3	8.4±2.7	9.84	8.448	-2.155	SB+
GJ 4231	21 52 10.4 05 37 35.7	Keck	2.4	14.6±2.7	13.62	8.248	-2.359	SB+
1RXS J221419.3+253411	22 14 17.66 25 34 06.6	Keck	4.3	23.9±2.7	11.33	10.177	-2.355	SB+
GJ 4282 (E)	22 33 22.65 -09 36 53.8 ^j	CFHT	2.5	26.7±4.1	9.91	8.534	-2.173	1.571" VB (Daemgen et al. 2007)
GJ 4282 (W)	22 33 22.65 -09 36 53.8	CFHT	2.6	26.7±4.1	9.91	8.534	-2.173	1.571" VB (Daemgen et al. 2007)
2MASS J22344161+4041387	22 34 41.62 40 41 38.8	Keck	6.0	30.9±4.3	14.24	12.573	-2.470	0.16" VB (Allers et al., in press), SB+

Table 1—Continued

Name ^a	RA & DEC J2000 (2MASS)	Tele- scope ^b	SpT M-(± 0.5) ^b	Dist. ^c (pc)	<i>I</i> <i>USNO</i>	<i>J</i> <i>2MASS</i>	$\log(F_X/F_J)$ ^d	Binarity ⁱ
LP 984-91	22 44 57.94 -33 15 01.6 ^j	Keck	4.5	23.7 \pm 2.0	13.51	7.786	-1.988	SB1
GJ 873	22 46 49.81 44 20 03.1	CFHT	3.2	5.1 \pm 0.0	8.88	6.106	-1.928	SB1
NLTT 54873	22 47 37.64 40 41 25.4 ^j	CFHT	3.8	21.7 \pm 2.7	11.44	10.35	-1.980	SB1
GJ 875.1	22 51 53.49 31 45 15.3 ^j	CFHT	2.7	14.3 \pm 0.6	10.5	7.697	-2.351	SB1
2MASS J22581643-1104170	22 58 16.43 -11 04 17.1	CFHT	2.7	23.0 \pm 3.7	10.27	9.071	-2.469	--
GJ 9809	23 06 4.83 63 55 34.0	CFHT	0.3	24.9 \pm 1.0 ^g	9.6	7.815	-2.281	SB1
NLTT 56194	23 13 47.28 21 17 29.4	Keck	7.5	20.2 \pm 2.7	13.03	11.421	-2.097	SB1
NLTT 56566	23 20 57.66 -01 47 37.3 ^j	CFHT	3.8	22.6 \pm 6.7	10.76	9.355	-2.362	0.099 ^h VB (Daemgen et al. 2007)
GJ 4338 B	23 29 22.58 41 27 52.2	CFHT	4.2	14.8 \pm 0.4 ^g	8.48	8.017	-2.041	SB1
GJ 4337 A	23 29 23.46 41 28 06.9	CFHT	2.9	14.8 \pm 0.4 ^g	10	7.925	-2.077	SB1
GJ 1290	23 44 20.84 21 36 05.0	CFHT	3.4	22.0 \pm 2.2 ^g	10.41	9.07	-2.406	SB1
1RXS J235005.6+265942	23 50 6.39 26 59 51.9 ^j	CFHT	4.0	26.5 \pm 4.3	11.22	10.142	-2.192	SB1
G 68-46	23 51 22.28 23 44 20.8 ^j	CFHT	4.0	18.1 \pm 3.3	10.79	9.683	-2.469	SB1
1RXS J235133.3+312720	23 51 33.67 31 27 23.0	CFHT	2.0	35.0 \pm 5.6	10.92	9.821	-2.228	SB1
1RXS J235452.2+383129	23 54 51.47 38 31 36.3	CFHT	3.1	13.2 \pm 2.1	10.22	8.937	-2.189	SB1
GJ 4381	23 57 49.9 38 37 46.9	CFHT	2.8	8.9 \pm 2.7	9.91	8.691	-2.206	SB1
G 273-191 (N)	23 58 13.66 -17 24 33.8 ^j	CFHT	1.9	26.1 \pm 2.0	9.72	8.311	-2.332	1.904 ^h VB (Daemgen et al. 2007), SB1
G 273-191 (S)	23 58 13.66 -17 24 33.8	CFHT	1.9	26.1 \pm 2.0	9.72	8.311	-2.332	1.904 ^h VB (Daemgen et al. 2007), SB1
G 130-31	23 59 19.86 32 41 24.5	Keck	5.6	23.9 \pm 2.7	11.8	10.451	-2.241	SB1

^aThose target names with directions in parentheses were resolved as visual binaries (VB) and when possible, both components were observed. If a target was resolved as a VB by another group (see last column) but not resolved at the telescope, the resulting spectrum is a composite of the both components. Likewise, the published photometry is of the combined system.

^bEach of the two spectrographs used, Keck+HIRES and CFHT+ESPaDOnS, produces a different measurement error for the TiO index and thus, the errors of the calculated SpTs are $\delta(\text{SpT}) = 0.33, 0.11$, respectively. However, the calibration is based on a sample binned to 0.5 subclasses, limiting the true uncertainty to this value.

^cPhotometric distances from Reid et al. (2002b, 2007a) unless otherwise noted. Daemgen et al. (2007) revised the distances to those VBs resolved by them. (See last column). Distances of those VBs resolved by us during acquisition have been corrected for their binarity assuming equal flux for each component.

^dFractional X-ray flux from the ROSAT All-Sky Survey. Three targets were not detected by ROSAT but have been included in the sample due to previously published indications of youth. (See column 7 of Table 2.)

^eDue to either poor S/N or bad seeing, we were unable to measure reliable TiO indices for these targets and defer to the published SpT (± 0.5 subclasses) based on low-resolution data (Reid et al. 2002b, 2007a).

^fNorton et al. (2007) attribute the photometric period to an eclipsing binary of BY Dra-type, however we see no evidence that this target is a spectroscopic binary.

^gDistances from the Hipparcos & Tycho Catalogues (Perryman & ESA 1997) using trigonometric parallaxes.

^hThese targets were plagued with poor seeing and/or low S/N *and* no previously published SpT. Therefore, we did a by-eye comparison of the TiO bands with spectra of known SpT. The error for these is ± 1 subclass.

ⁱVisual binaries are marked as “VB”. Stars observed during two epochs with no RV variation are marked as “SB1”.

^jLow-resolution spectra were obtained of these targets by Riaz et al. (2006).

Table 2. Measured Quantities and Stellar Ages

Name	SpT M- (± 0.5)	CaH ^a wide	CaH ^a narr	K I EW ^a (Å)	H α EW ^a (Å)	Youth ^b Index	Youth Indicator from literature	Age ^c (Myr)
2MASS J00034227-2822410	7.0	—	—	2.35	-2.19	?0000	—	100-300
G 217-32	3.8	1.45	1.65	0.91	-3.42	01000	—	35-300
LP 348-40	3.5	1.26	1.40	1.01	0.13	11000	—	\gtrsim 2000
NLTT 614	6.4	1.36	1.53	1.94	-9.42	10100	—	90-300
1RXS J001557.5-163659	4.1	1.43	1.61	1.91	-4.36	00100	—	35-300
GJ 1006 A	3.6	1.22	1.43	0.83	-2.70	11000	—	35-300
GJ 3030	2.4	1.25	1.36	1.84	-2.00	10000	—	20-150
GJ 3036	3.7	1.39	1.57	1.05	-4.56	01000	—	35-300
NLTT 1875	4.3	1.31	1.47	1.42	-2.63	10000	—	40-300
G 69-32	4.6	1.34	1.54	1.06	-5.48	11000	—	60-300
G 132-51B (W)	2.6	1.30	1.41	0.99	-2.46	11000	—	20-150
G 132-51B (E)	3.8	1.39	1.56	1.04	-4.78	01000	—	35-300
G 269-153 (NE)	4.3	1.42	1.60	1.76	-6.62	01000	—	40-300
G 269-153 (SW)	4.6	1.44	1.61	1.82	-6.77	00000	—	60-300
G 172-56	5.4	1.46	1.68	1.09	-9.72	00000	—	60-300
2MASS J01351393-0712517	4.3	1.34	1.50	1.30	-5.36	10000	—	40-300
G 271-110	3.5	1.40	1.58	1.79	-5.03	00000	—	25-300
LHS 6032 (SW)	1.3	1.23	1.32	1.35	-2.35	00000	—	15-150
1RXS J015027.1-185134	5.4	1.42	1.64	2.49	-8.35	00000	—	60-300
NLTT 6549	1.5	1.21	1.31	0.89	-2.16	11000	—	15-150
GJ 1041A (SW)	0.6	1.11	1.16	0.68	0.59	11000	—	15-150 ^d
GJ 82	4.2	1.35	1.50	1.57	-4.37	10000	—	35-300
GJ 3136	2.9	1.35	1.49	1.30	-5.63	00000	flare star (Gershberg et al. 1999)	20-300
1RXS J021836.6+121902	1.9	1.22	1.33	0.84	-1.45	11000	—	20-150
GJ 3150	3.6	1.42	1.59	1.84	-5.48	00000	—	35-300
1RXS J022735.8+471021	4.6	1.50	1.65	2.03	-8.85	00000	—	60-300
1RXS J023138.7+445640	4.4	1.33	1.47	1.08	-5.11	11000	—	40-300
G 36-26	5.9	1.43	1.62	2.21	-3.45	10000	—	90-300
GJ 3174	3.7	1.35	1.51	1.85	-2.40	10000	—	35-300
LP 247-13	2.7	1.29	1.41	0.89	-3.99	11000	weak-line T Tau? (Li & Hu 1998)	20-100
G 246-33	4.1	1.44	1.60	2.12	-4.65	00000	—	35-300
1RXS J032230.7+285852	4.0	1.31	1.47	1.81	-8.14	10000	—	35-300
2MASS J03350208+2342356	8.5	1.29	1.43	3.15	-10.72	11111	Li detection (Reid et al. 2002b)	10
1RXS J034231.8+121622	5.2	1.42	1.68	1.48	-5.66	00000	—	60-300

Table 2—Continued

Name	SpT M- (± 0.5)	CaH ^a wide	CaH ^a narr	K I EW ^a (Å)	H α EW ^a (Å)	Youth ^b Index	Youth Indicator from literature	Age ^c (Myr)
G 80-21	2.8	1.33	1.54	0.81	-2.76	01000	AB Dor member (Zuckerman et al. 2004)	30-50
II Tau	4.6	1.42	1.69	1.87	-7.22	00000	Pleiades member (Stauffer et al. 1991)	120
1RXS J041325.8-013919	5.3	1.44	1.69	1.79	-9.00	00000	—	60-300
1RXS J041417.0-090650	4.3	1.50	1.79	1.67	-14.15	00110	—	<40
GJ 3287	3.8	1.38	1.55	1.47	-2.04	00000	flare star (Gershberg et al. 1999)	35-300
GJ 3305	1.1	1.20	1.36	0.79	-2.10	01010	β Pic member (Torres et al. 2006)	12
GJ 3304	4.6	1.50	1.79	1.97	-4.40	00000	—	60-300
NLTT 13728	6.0	1.62	1.90	2.75	-19.11	00111	—	<90
NLTT 13837	4.3	1.52	1.80	1.79	-4.90	00000	—	40-300
NLTT 13844	4.6	1.42	1.74	2.06	-3.63	00000	—	60-300
2MASS J04465175-1116476	4.9	1.63	1.98	1.09	-4.11	01000	—	60-300
2MASS J04472312-2750358	0.5	1.14	1.28	0.75	0.47	01000	—	$\gtrsim 400$
G 81-34	4.0	1.37	1.52	1.86	-3.30	10000	—	35-300
1RXS J045101.0+312734	3.7	1.43	1.70	1.39	-2.31	00000	—	35-300
NLTT 14116	3.3	1.36	1.58	1.32	-6.96	00000	AB Dor member (Torres et al. 2008)	30-50
GJ 3335	3.5	1.31	1.49	1.07	-3.08	11000	—	25-300
NLTT 15049	3.8	1.43	1.68	1.56	-2.91	00000	—	35-300
GJ 207.1	2.0	1.35	1.64	1.53	-4.96	00000	flare star (Gershberg et al. 1999)	20-150
1RXS J055446.0+105559	2.1	1.28	1.39	0.53	-3.31	11000	—	20-150
2MASS J05575096-1359503	7.0	1.15	1.49	0.13	-25.56	11011	mis-classified as giant (Cruz et al. 2007)	10
GJ 3372 B	4.2	1.42	1.58	1.60	-3.38	00000	—	40-300
G 249-36	4.9	1.32	1.52	1.26	-6.11	10100	—	60-300
GJ 3395	0.8	1.17	1.26	0.59	-1.46	01000	—	20-150
G 108-36	2.5	1.27	1.40	0.78	-0.18	11000	—	20-150 ^d
GJ 3417 (NE)	5.2	1.36	1.52	0.26	-3.06	11000	—	60-300
GJ 2060	1.3	1.24	1.41	0.88	-3.10	01000	AB Dor member (Zuckerman et al. 2004)	30-50
GJ 277B	3.3	1.26	1.39	1.57	-2.20	10000	—	25-300
1RXS J073829.3+240014	2.7	1.35	1.51	1.88	-3.78	00000	—	20-300
NLTT 18549	7.0	1.46	1.63	2.81	-22.26	10101	strong H α emission (Cruz et al. 2003)	100
2MASS J07572716+1201273	2.3	1.28	1.46	0.93	-0.32	01000	—	$\gtrsim 1200$
2MASS J08031018+2022154	3.3	1.41	1.64	1.57	-6.10	00000	—	25-300
GJ 316.1	6.0	1.59	1.96	3.46	-22.68	00101	—	100
NLTT 20303	2.6	1.31	1.57	1.15	-2.93	00000	—	20-300
1RXS J091744.5+461229	1.7	1.25	1.40	1.04	-3.89	01000	—	20-150

| 30 |

Table 2—Continued

Name	SpT M- (± 0.5)	CaH ^a wide	CaH ^a narr	K I EW ^a (Å)	H α EW ^a (Å)	Youth ^b Index	Youth Indicator from literature	Age ^c (Myr)
G 43-2	2.0	—	—	1.94	-2.13	?0000	—	20-150
NLTT 22741	4.5	—	—	2.02	-4.98	?0100	100–200 Myr (Reid & Walkowicz 2006)	40-300
GJ 3577 A (W)	3.5	—	—	1.98	-6.07	?0000	—	25-300
G 196-3A	3.0	—	—	1.07	-3.77	?0000	—	25-300
GJ 2079	0.7	—	—	1.11	-0.99	?1000	—	\gtrsim 400
1RXS J101432.0+060649	4.1	—	—	1.38	-4.09	?0000	—	35-300
GJ 388	3.5	—	—	1.39	-2.99	?0000	—	25-300
G 44-9	5.9	—	—	1.13	-5.30	?0000	—	90-300
2MASS J10364483+1521394	4.0	—	—	2.07	-4.99	?0000	—	35-300
GJ 3629	3.0	—	—	1.25	-3.07	?0000	—	25-300
GJ 3639	3.5	—	—	2.05	-4.80	?0000	—	25-300
NLTT 26114	3.0	—	—	1.85	-2.56	?0000	—	25-300
G 119-62	3.5	—	—	1.80	-3.79	?0000	—	25-300
1RXS J111300.1+102518	3.0	—	—	1.61	-3.11	?0000	—	25-300
GJ 3653	0.5	—	—	0.90	-2.06	?1000	—	15-150
2MASS J11240434+3808108	4.5	—	—	1.74	-3.19	?0000	—	40-300
G 10-52	3.5	—	—	1.54	-4.36	?0000	—	25-300
2MASS J12065663+7007514 (E)	4.4	1.35	1.48	1.71	-0.17	10000	—	\gtrsim 4500
G 122-74	3.5	—	—	0.94	0.37	?0000	—	\gtrsim 2000
GJ 3729	3.5	—	—	1.88	-2.23	?0000	—	25-300
GJ 3730	4.0	—	—	1.27	-1.42	?0000	—	35-300
1RXS J124147.5+564506	2.5	—	—	1.67	-3.67	?0000	—	20-150
GJ 490 B	4.0	—	—	2.20	-4.06	?0000	—	35-300
GJ 490 A	0.5	—	—	1.05	-1.29	?1000	—	15-150
NLTT 32659 (E)	3.7	1.29	1.48	1.66	-3.69	10000	—	35-300
NLTT 32659 (W)	1.6	1.18	1.32	0.74	-2.26	11000	—	20-150
GJ 1167 A	4.8	1.40	1.62	2.66	-4.82	00000	flare star (Gershberg et al. 1999)	60-300
GJ 3786	3.5	—	—	2.11	-3.43	?0000	—	25-300
2MASS J13292408–1422122	2.8	1.33	1.48	1.44	-3.08	00000	—	20-150
2MASS J14215503–3125537	3.9	1.29	1.48	1.55	-6.36	10100	—	35-300
2MASS J1442809–0424078	3.0	1.31	1.50	1.29	-4.63	00000	—	20-150
1RXS J150907.2+590422	2.2	1.29	1.41	1.09	-2.55	01000	—	20-150
GJ 9520	1.0	1.14	1.27	0.76	-2.14	01000	—	15-150
NLTT 40561	3.5	1.30	1.47	1.57	-7.27	10100	—	25-300

Table 2—Continued

Name	SpT M- (± 0.5)	CaH ^a wide	CaH ^a narr	K I EW ^a (Å)	H α EW ^a (Å)	Youth ^b Index	Youth Indicator from literature	Age ^c (Myr)
G 167-54	4.1	1.33	1.58	2.70	-0.70	10000	—	$\gtrsim 4500$
2MASS J15534211-2049282 (S)	3.4	1.23	1.41	0.55	-78.35	11111	low g (I.N. Reid, priv. comm.)	3
GJ 3928	5.3	1.37	1.51	2.11	-5.94	10100	—	60-300
NLTT 43695 (E)	4.6	1.27	1.51	1.88	-3.19	10000	—	60-300
LP 331-57	2.4	1.30	1.43	1.45	-1.62	00000	—	20-150
GJ 616.2	5.6	1.33	1.58	2.31	-7.43	10000	—	90-300
GJ 669A	3.4	1.23	1.43	1.56	-0.90	10000	—	$\gtrsim 2000$
1RXS J173130.9+272134	2.6	—	—	4.89	-7.31	70000	—	20-300
G 227-22	6.1	1.52	1.76	2.51	-7.70	00000	—	90-300
GJ 4044	4.5	1.42	1.64	1.98	-6.99	00000	flare star (Gershberg et al. 1999)	40-300
LP 390-16	3.8	1.38	1.55	1.79	-4.34	00000	—	35-300
1RXS J183203.0+203050 (N)	4.9	1.40	1.63	2.61	-3.14	00000	—	60-300
1RXS J183203.0+203050 (S)	5.1	1.47	1.71	2.29	-10.92	00000	—	60-300
1RXS J184410.0+712909 (E)	3.9	1.37	1.53	1.59	-5.24	00100	—	35-300
1RXS J184410.0+712909 (W)	4.1	1.43	1.70	2.15	-3.17	00000	—	35-300
GJ 9652 A	4.5	1.34	1.55	1.60	-5.71	10000	—	60-300
2MASS J19303829-1335083	6.0	1.38	1.57	3.06	-4.90	10000	—	90-300
1RXS J193124.2-213422	2.4	1.21	1.36	1.24	-5.36	10000	—	20-150
1RXS J193528.9+374605	3.0	1.25	1.45	1.60	-2.58	10000	—	20-300
1RXS J194213.0-204547	5.1	1.38	1.58	2.34	-6.49	10000	—	60-300
G 125-36	2.1	1.22	1.39	1.13	-0.24	00000	—	$\gtrsim 1200$
2MASS J20003177+5921289	4.1	1.43	1.64	1.87	-5.67	00000	—	35-300
1RXS J204340.6-243410 (NE)	3.7	1.23	1.37	0.73	-5.24	11000	—	35-300
1RXS J204340.6-243410 (SW)	4.1	1.31	1.49	0.79	-8.03	11000	—	35-300
NLTT 49856	4.5	1.37	1.63	1.76	-6.50	00100	—	40-300
2MASS J20530910-0133039	5.6	1.53	1.85	1.92	-3.15	00000	—	90-300
NLTT 50066	2.9	1.32	1.50	1.38	-2.57	00000	—	20-300
GJ 4185B	3.3	1.31	1.49	1.49	-3.21	00000	—	25-300
GJ 4185 A	3.3	1.32	1.51	1.77	-5.50	00100	—	25-300
GJ 4231	2.4	1.21	1.37	1.22	-4.19	10000	—	20-150
1RXS J221419.3+253411	4.3	1.38	1.59	1.70	-5.53	00000	—	40-300
GJ 4282 (E)	2.5	1.33	1.47	1.02	-4.41	01000	—	20-150
GJ 4282 (W)	2.6	1.32	1.45	1.09	-4.94	01000	—	20-150
2MASS J22344161+4041387	6.0	1.20	1.27	0.14	-46.00	11011	low g, strong H α (Cruz et al. 2003, Allers et al. 2009)	~ 1

Table 2—Continued

Name	SpT M- (± 0.5)	CaH ^a wide	CaH ^a narr	K I EW ^a (Å)	H α EW ^a (Å)	Youth ^b Index	Youth Indicator from literature	Age ^c (Myr)
LP 984-91	4.5	1.33	1.50	0.62	-7.80	11000	β Pic member (Torres et al. 2006)	12
GJ 873	3.2	1.36	1.52	1.59	-3.63	00000	flare star (Gershberg et al. 1999)	25-300
NLTT 54873	3.8	1.39	1.55	1.79	-3.27	00100	—	35-300
GJ 875.1	2.7	1.29	1.41	1.30	-3.38	10000	—	20-300
2MASS J22581643-1104170	2.7	1.29	1.42	1.37	-1.22	10000	—	20-300
GJ 9809	0.3	1.12	1.18	1.00	-1.27	01010	AB Dor member, Li detection (Zuckerman et al. 2004)	30-50
NLTT 56194	7.5	1.35	1.54	2.72	-7.92	10000	—	100-300
NLTT 56566	3.8	1.34	1.47	1.65	-4.18	10000	—	35-300
GJ 4338 B	4.2	1.41	1.55	2.00	-5.05	00000	flare star (Gershberg et al. 1999)	40-300
GJ 4337 A	2.9	1.30	1.42	1.47	-3.48	10000	—	20-300
GJ 1290	3.4	1.32	1.46	1.59	-1.69	10000	—	25-300
1RXS J235005.6+265942	4.0	1.45	1.62	1.76	-6.07	00000	—	35-300
G 68-46	4.0	1.38	1.54	1.53	-5.69	00000	—	35-300
1RXS J235133.3+312720	2.0	1.25	1.36	1.35	-2.82	10000	—	20-150
1RXS J235452.2+383129	3.1	1.35	1.51	1.53	-3.39	00000	—	25-300
GJ 4381	2.8	1.31	1.45	1.46	-3.73	00000	—	20-300
G 273-191 (N)	1.9	1.24	1.35	1.10	-3.26	11000	—	20-150
G 273-191 (S)	1.9	1.24	1.36	1.04	-2.98	01000	—	20-150
G 130-31	5.6	1.27	1.44	1.83	-6.61	10000	—	90-300

^aEach of the two spectrographs used, Keck+HIRES and CFHT+ESPaDOnS, produces different error bars for measured values. As discussed in Section 4, the smaller errors for the CFHT data are due to the more stable fiber-fed instrumental set-up of ESPaDOnS. (See Table 1.) The measurement errors for Keck and CFHT respectively are: $\delta(\text{CaH-wide}) = 0.035, 0.008$, $\delta(\text{CaH-narr}) = 0.051, 0.013$, $\delta(\text{K I EW}) = 0.24, 0.16$, $\delta(\text{H}\alpha \text{ EW}) = 0.45, 0.21$. Negative H α EWs indicate the line is in emission.

^bYouth index in binary format in order of least to most restrictive age indicator: low-g from CaH, low-g from K I, He I emission, Li detection, strong H α emission (EW_{H α} < -10 Å). Note that determining low-g targets of SpT \gtrsim M6 from the CaH and KI indicators is difficult unless extremely young. See Section 5.1 for more details. Also, due to either poor S/N or bad seeing, we were unable to measure reliable CaH indices from those spectra (denoted by a '?').

^cAge limits are based on youth diagnostics discussed in Section 5, unless a target has been previously published to be a member of known young moving group, in which case the age of the group is adopted. For stars with no additional indications of youth, the lower limit is based on the lack of lithium in the spectra and the upper limit is the *statistical* age determined from their SpT and X-ray emission, i.e. A star of SpT earlier than M2.5 has an upper age limit of 150 Myr and one of later SpT 300 Myr. For the 11 stars with no significant H α emission (i.e. > -1 Å), we list their activity lifetimes (≥ 400 Myr) as determined by West et al. (2008). These ages have large error bars on the order of 500 Myr.

^dP 348-40, GJ 1041A (SW) and G 108-36 appear to have low surface gravity using both the CaH and K I diagnostics but do not have any H α emission. According

to West et al. (2008), the lack of H α implies an age > 2000, 400 and 1200 (± 400) Myr, respectively.

Table 3. RV Standards

Name	Tele-scope ^a	SpT M– ±0.5	J 2MASS	log(F_X/F_J)	CaH ^a wide	CaH ^a narr	K I ^a Å	H α ^a Å	[Fe/H] ^b publ.	[Fe/H] ^b J&A ^c	RV Source ^b
GJ 406	Keck	6.0	7.085	-2.928	1.50	1.69	3.45	-9.03	–	high	[4]
LHS 2065	Keck	9.0	11.212	-3.336	1.09	1.21	1.94	-30.49	–	–	[5]
GJ 436	Keck	2.7	6.900	–	1.25	1.39	1.02	0.46	+0.02±0.20 [1]	high	[4]
GJ 179	CFHT	3.7	7.814	–	1.27	1.38	1.36	0.09	+0.02±0.30 [2]	high	[6]
GJ 908	CFHT	1.3	5.827	-4.110	1.15	1.25	0.91	0.40	-0.52±0.20 [1]	low	[4]
VB 10	Keck	8.0	9.908	–	1.39	1.61	3.57	-4.29	-0.05±0.20 ^c [1]	–	[7]
GJ 205	CFHT	1.2	4.999	-3.972	1.16	1.25	0.81	0.46	+0.21±0.13 [3]	high	[6]
GJ 687	CFHT	3.2	5.335	-4.347	1.24	1.36	1.15	0.16	+0.15±0.09 [3]	high	[4]
GJ 821	CFHT	1.0	7.688	–	1.16	1.27	0.75	0.54	-0.65±0.30 [2]	low	[4]
GJ 273	CFHT	3.8	5.714	–	1.28	1.41	1.25	0.00	-0.16±0.20 [1]	solar	[4]

^aEach of the two spectrographs used, Keck+HIRES and CFHT+ESPaDOnS, produces different error bars for the CaH indices and K I and H α EWs. (See Table 1.) The errors for Keck and CFHT respectively are: $\delta(\text{CaH-wide}) = 0.035, 0.008$, $\delta(\text{CaH-narr}) = 0.051, 0.013$, $\delta(\text{K I EW}) = 0.24, 0.16$, $\delta(\text{H}\alpha \text{ EW}) = 0.45, 0.21$.

^bReferences: [1] Bonfils et al. (2005), [2] Casagrande et al. (2008), [3] Woolf & Wallerstein (2005), [4] Nidever et al. (2002), [5] Reid et al. (2002b), [6] Marcy & Benitz (1989).

^cAs discussed in the text, Johnson & Apps (2009) have shown that [Fe/H] determinations using the Bonfils et al. (2005), and thus the Casagrande et al. (2008), calibration are strongly underestimated. Here we have indicated whether the RV standard has higher or lower than solar metallicity using the new Johnson & Apps photometric calibration (Figure 8). Those that are left blank have colors beyond the limits of the new calibration, which is valid for $3.9 < (V-K) < 6.6$.

^dBased on metallicity measurement for VB 10's companion M dwarf, GJ 752A.

Table 4. Observed β Pic Members

Name	RA & DEC	M subclass ± 0.5	J <i>2MASS</i>	$\log(F_X/F_J)$	CaH wide, ± 0.008	CaH narr, ± 0.013	K I EW $\pm 0.16 \text{ \AA}$	H α EW $\pm 0.21 \text{ \AA}$	Li EW ^a $\pm 0.025 \text{ \AA}$	Youth ^b Index
AU Mic	20 45 9.5 -31 20 27	0.9	5.436	-2.125	1.13	1.20	0.96	-1.41	0.074	11010
AT Mic (N)	20 41 51.1 -32 26 7	4.5	5.807	-2.195	1.37	1.52	0.87	-11.04	–	11101
AT Mic (S)	20 41 51.1 -32 26 10	4.9	5.807	-2.195	1.38	1.55	1.08	-8.13	–	11100
BD+30 397B	2 27 28.1 +30 58 41	2.2	8.817	-1.821	1.24	1.36	0.89	-3.95	0.133	11010
BD-13 6424	23 32 30.9 -12 15 52	0.8	7.45	-2.311	1.14	1.21	0.75	-1.83	0.171	11010
GJ 182	4 59 34.8 +1 47 2	0.5	7.117	-2.450	1.12	1.18	0.74	-1.23	0.257	11010
HIP 11437 B	2 27 28.1 +30 58 41	-0.2	8.817	-1.821	1.04	1.07	0.53	-0.16	0.271	11010
HIP 12545	2 41 25.8 +5 59 19	-0.1	7.904	-2.203	1.06	1.09	0.59	-0.69	0.447	11010

^aThe lithium abundances have not been corrected for possible contamination with the Fe I line at 6707.44 \AA . Uncertainties in the setting of continuum levels prior to measurement induce EW errors of about 10–20 m \AA (Zuckerman & Song 2004) with a strong dependence on the S/N in the region. We therefore conservatively consider our detection limit to be 0.05 \AA .

^bYouth index in binary format in the following order: low-g from CaH, low-g from K I, He I emission, Li detection, strong H α emission ($\text{EW}_{\text{H}\alpha} < -10 \text{ \AA}$).

Table 5. Targets with detected lithium

Name	SpT M– (± 0.5)	Li EW ^a $\pm 0.025 \text{ \AA}$	He I EW $\pm 0.05 \text{ \AA}$	H α EW $\pm 0.45 \text{ \AA}$	H α 10%-width $\pm 4 \text{ km/s}$	Accretor? ^b
2MASS J03350208+2342356	8.5	0.615	–2.89	–10.7	273	yes
2MASS J05575096–1359503	7.0	0.285	–	–25.6	208	possible
2MASS J15534211–2049282 (S)	3.4	0.630	–0.81	–70.9, –85.8	421, 470	yes
2MASS J22344161+4041387	6.0	0.825	–	–52.7, –39.2	314, 298	yes
1RXS J041417.0–090650	4.3	0.078	–0.54	–5.1, –23.2	86, 242	no
GJ 3305	1.1	0.086	–	–2.1	113	no
GJ 9809	0.3	0.087	–	–1.3	105	no
NLTT 13728	6.0	0.126	–0.28	–19.1	89	no

^aThe lithium abundances have not been corrected for possible contamination with the Fe I line at 6707.44 Å. Uncertainties in the setting of continuum levels prior to measurement induce EW errors of about 10–20 mÅ (Zuckerman & Song 2004) with a strong dependence on the S/N in the region. We therefore consider our detection limit to be 0.05 Å.

^bAccreting or not, based on criteria discussed in text and devised by Mohanty et al. (2005) and White & Basri (2003).

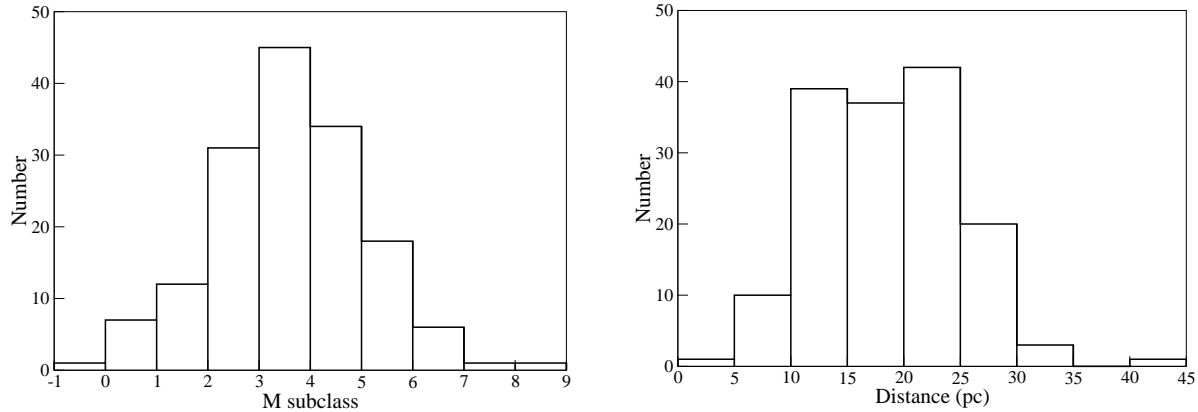


Fig. 1.— Spectral type and distance histograms of the ROSAT-selected sample of M dwarfs. Distance greater than 25 pc (within error bars) are due to subsequent discoveries of visual binaries.

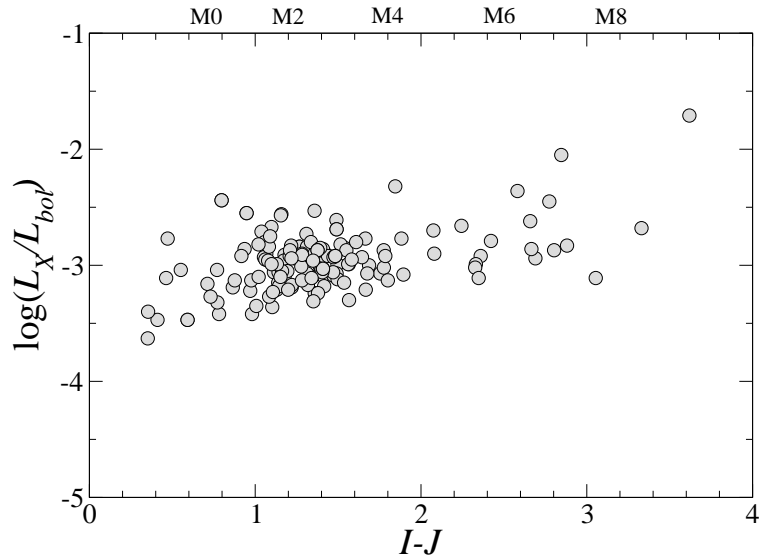


Fig. 2.— The fractional X-ray luminosity (L_X/L_{bol}) as a function of $I - J$ for our sample of single low-mass star.

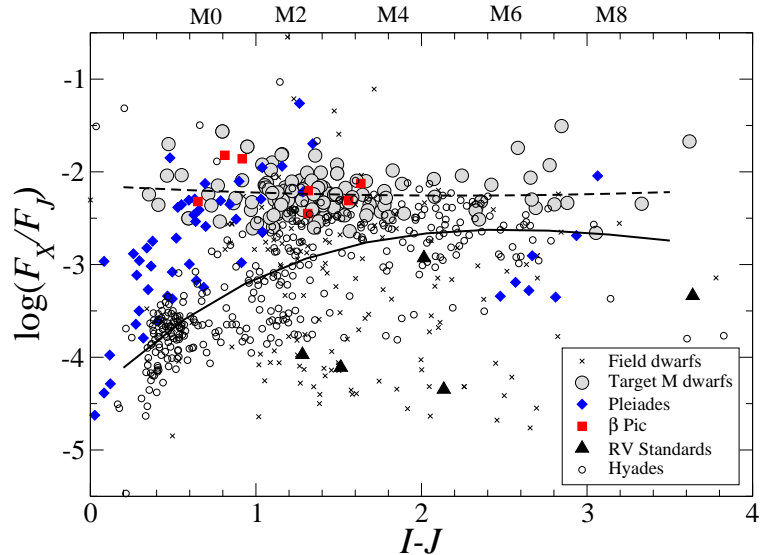


Fig. 3.— The fractional X-ray luminosity as a function of $I - J$ for our sample of single low-mass stars compared with seven M-dwarf members of the β Pic young moving group at 12 Myr (Torres et al. 2006), Pleiades members at 120 Myr (Micela et al. 1998), Hyades M dwarfs at 650 Myr (Stern et al. 1995), field stars (Hünsch et al. 1999), and the RV standard stars we observed that have been detected by ROSAT. The lines are quadratic fits to the M dwarf (dashed) and Hyades (solid) samples.

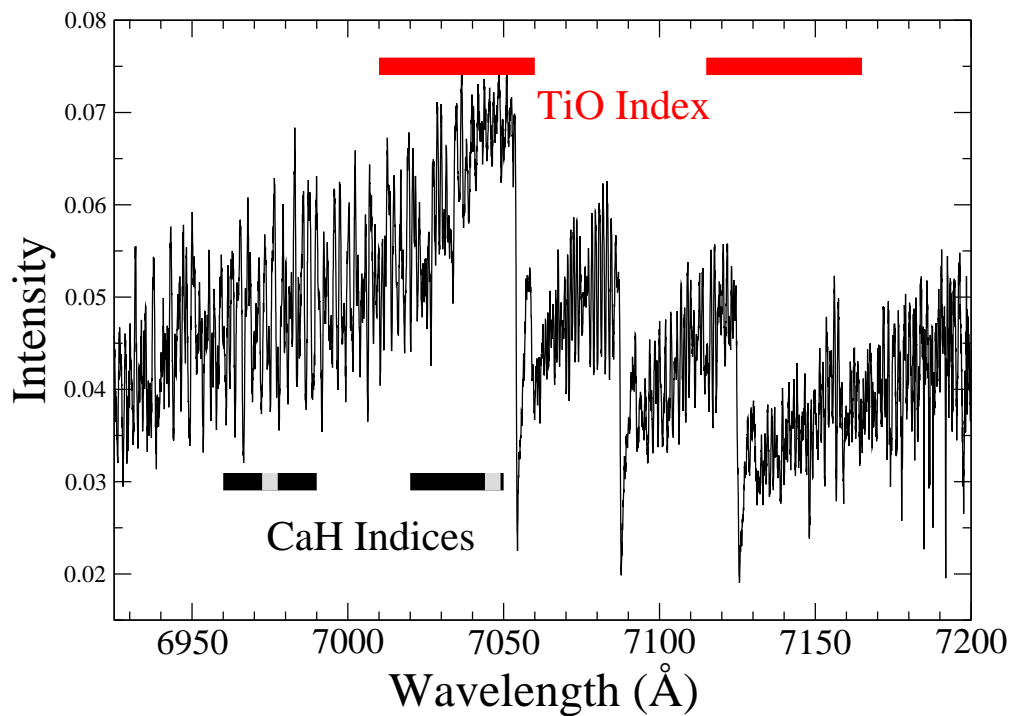


Fig. 4.— A single order of a CFHT/ESPaDoNS spectrum of GJ 875.1 (SpT=M3). The three indices discussed in the text are marked by the bars: TiO-7140: [7010–7060]/[7115–7165] (red), CaH-wide: [7020–7050]/[6960–6990] (blue), and CaH-narrow: [7044–7049]/[6972.5–6977.5] (green).

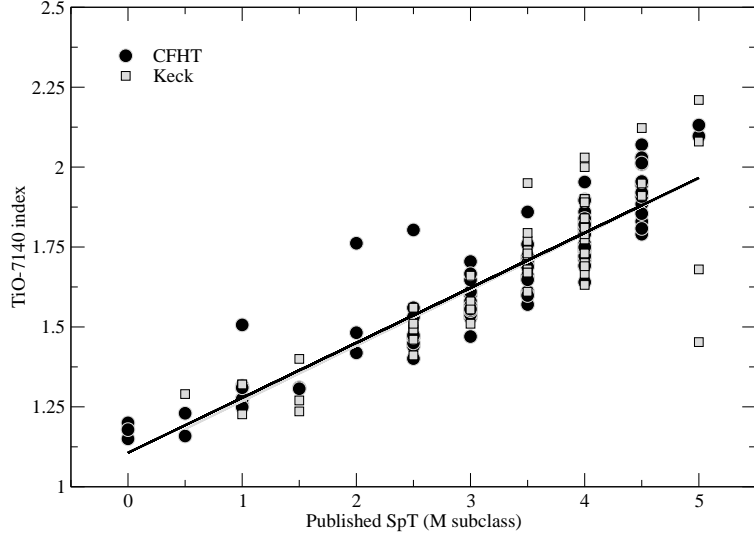


Fig. 5.— Calibration of the TiO-7140 index using published SpTs for those stars in our sample, plus a few RV standards and known β Pic members. The best-fit line to the CFHT data is virtually indistinguishable from that to the Keck data. The best fit to full data set results in a calibration of $\text{SpT} = (\text{TiO}_{7140} - 1.0911)/0.1755$.

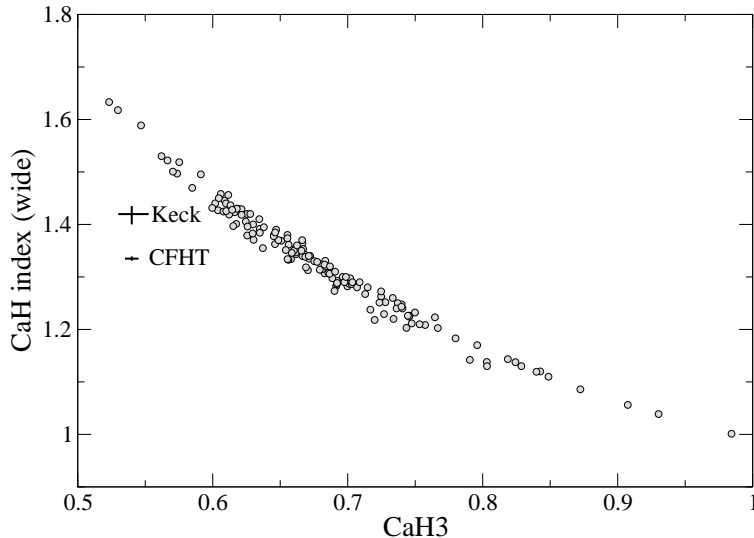


Fig. 6.— Correlation of the CaH3 index for Reid et al. (1995) and CaH (wide) of Kirkpatrick et al. (1991). See text for their definitions.

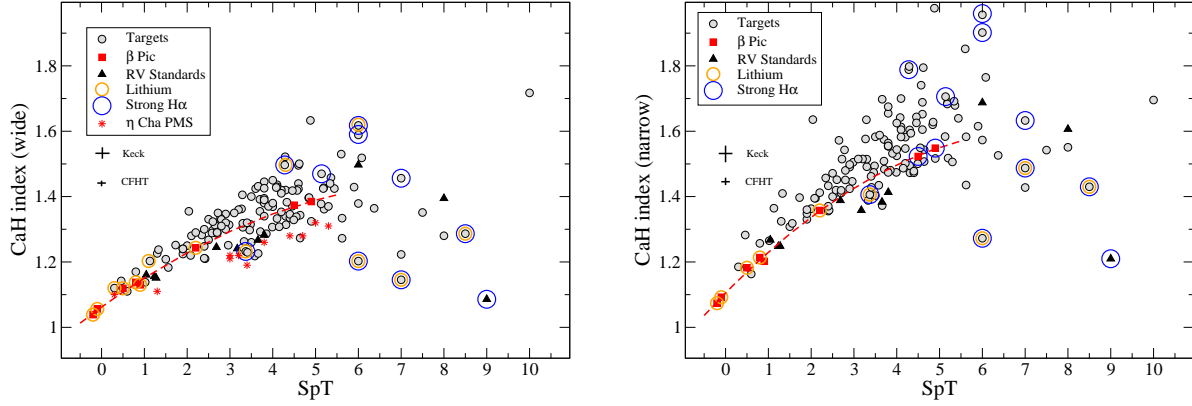


Fig. 7.— Surface gravity sensitive indices, CaH (wide; Kirkpatrick et al. 1991) and CaH (narrow; this work) as a function M-type subclasses. The red dashed curves are polynomial fits to our observations of β Pic M dwarfs: $\text{CaH}_{\text{wide}} = -0.0067 \text{ SpT}^2 + 0.0986 \text{ SpT} + 1.0633$ and $\text{CaH}_{\text{narr}} = -0.00891 \text{ SpT}^2 + 0.13364 \text{ SpT} + 1.1053$, respectively. The values in the left figure for the η Cha PMS cluster members (9 Myr) were measured from low-resolution ($R \approx 900$) spectra provided by Lyo et al. (2004).

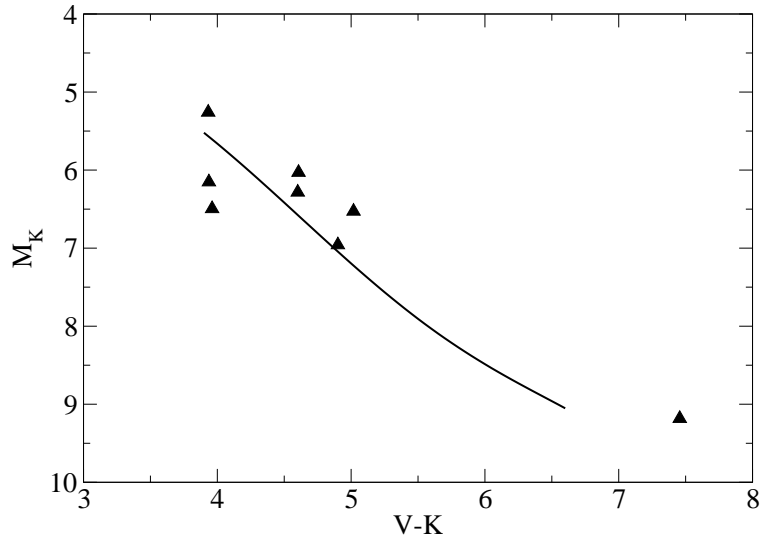


Fig. 8.— Color-magnitude plot for the RV standards. The solid line is the Johnson & Apps (2009) mean main-sequence. Those stars above the line are metal rich, while those below are metal poor.

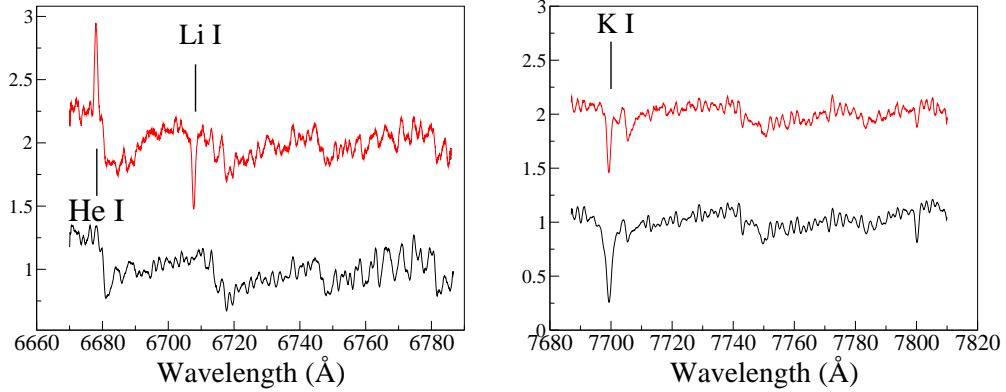


Fig. 9.— Two orders of Keck/HIRES spectra for two young M4 targets from our sample, 2MASS J1553 (S) (red) and 1RXS J142155.3 (black). *Top spectra*: The strong Li I ($\lambda 6708$) absorption, He I ($\lambda 6678$) emission, and the lower K I ($\lambda 7700$) EW all indicate a very young age for 2MASS J1553 (S), $\lesssim 40$ Myr based on Chabrier et al. (1996) models for pre-main sequence lithium depletion. *Bottom spectra*: 1RXS J142155.3 shows no clear spectroscopic signatures of low gravity, indicating it is on or near the main-sequence. However, its X-ray flux is significantly enhanced compared to Hyades stars and nearby (many Gyr old) field stars, indicating an age of $\lesssim 300$ Myr.

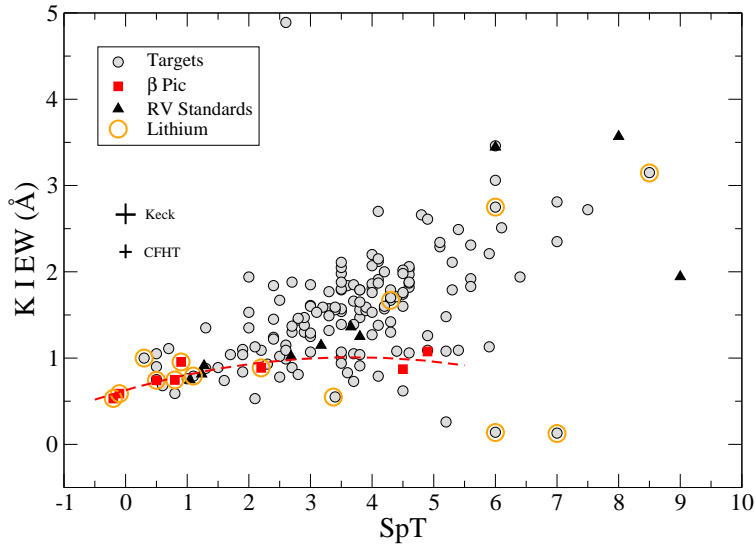


Fig. 10.— K I equivalent width as a function of M-type subclass. The red dashed curve is a polynomial fit to the β Pic observations: $EW_{KI} = -0.02821 \text{ SpT}^2 + 0.20731 \text{ SpT} + 0.62911$.

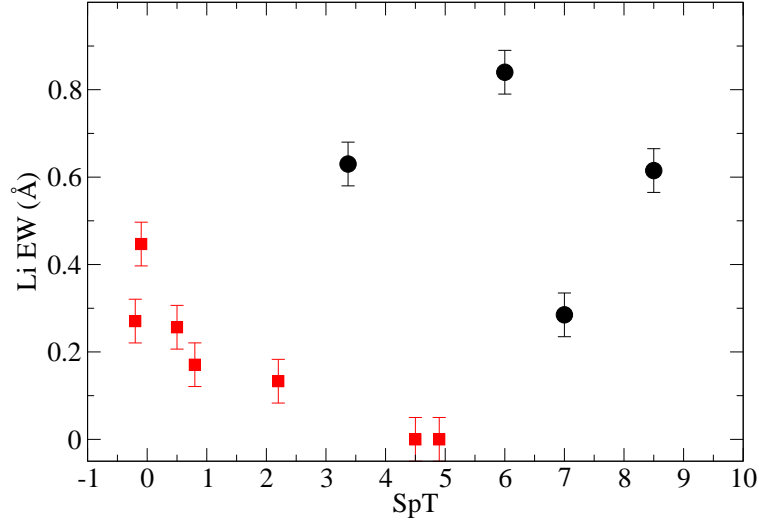


Fig. 11.— Measured lithium EWs for the 8 targets with clear Li absorption (black circles) and for the known β Pic members (red squares) that we observed.

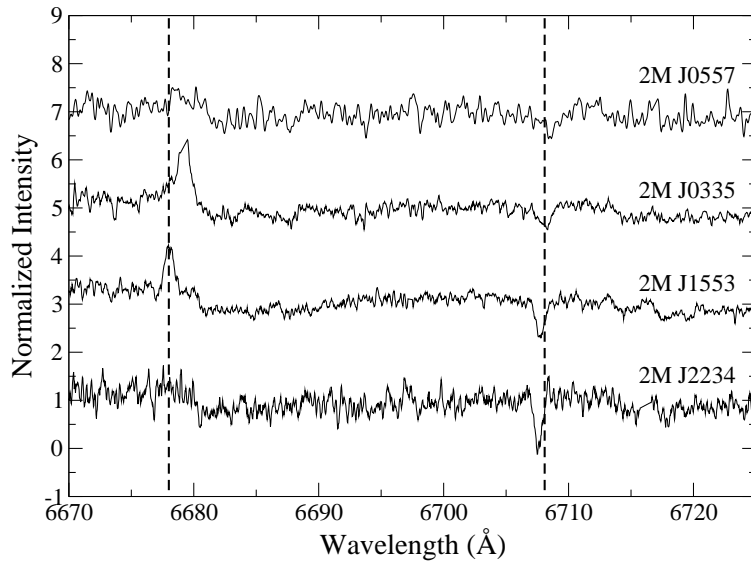


Fig. 12.— Keck/HIRES spectra of the four accreting targets listed in Table 5. The vertical dashed lines mark the rest wavelengths of He I (λ 6678) and Li I (λ 6708). The shifts of the Li line centers are due to the stars' radial velocities.

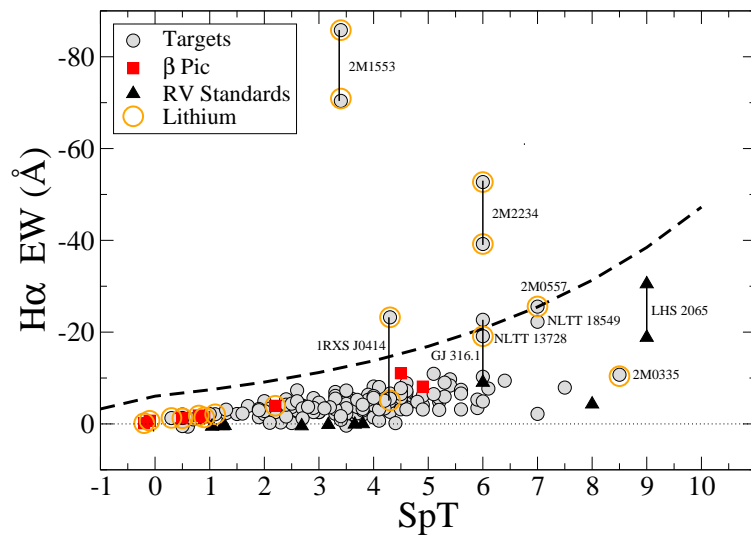


Fig. 13.— Measured $\text{EW}_{\text{H}\alpha}$. Of the 65 M dwarfs observed twice, 4 had $\text{H}\alpha$ variability in excess of 10 Å, plus the standard star LHS 2065. Each is plotted twice and connected with a solid line. The dashed curve represents the empirical accretion boundary determined by Barrado y Navascués & Martín (2003). See text for further discussion of the labeled targets.

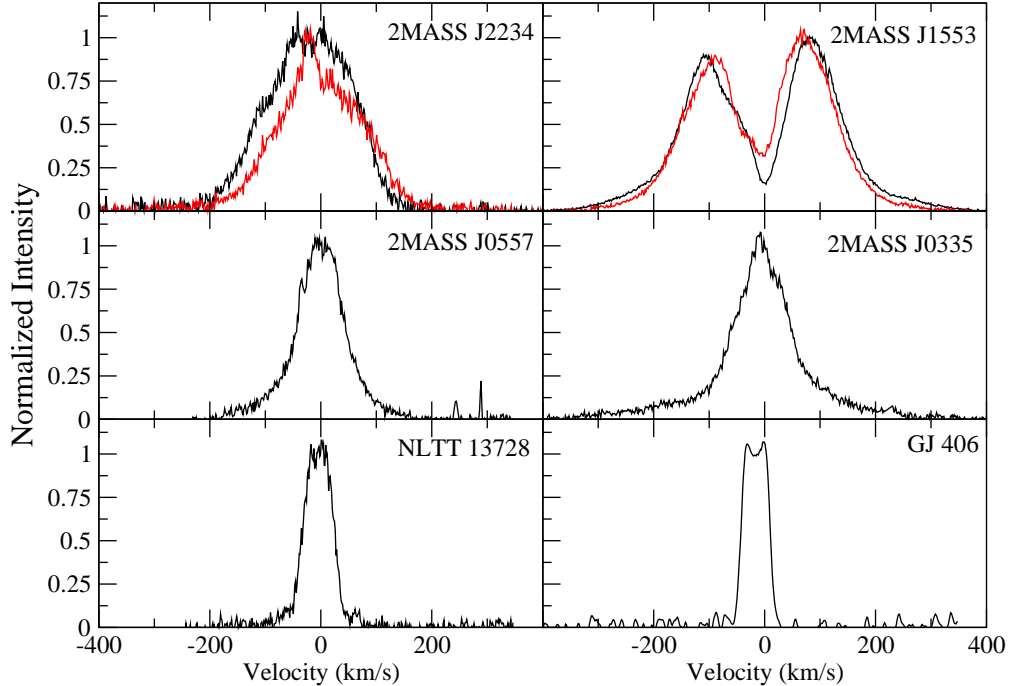


Fig. 14.— The top four H α velocity profiles are those of the targets with strong lithium absorption, while NLTT 13728 has weaker EW_{Li} and GJ 406, a RV standard, has none. Both observations are shown for 2MASS J2234 and 2MASS J1553. The profiles have been continuum-subtracted and normalized to range from 0.0 (continuum level) to 1.0 (emission peak level). Their 10%-widths (the full velocity span at 0.1 of the peak flux) are 306, 446, 207, 273, 89 and 72 km/s, top left to bottom right. According to criteria devised by White & Basri (2003) and Mohanty et al. (2005), 2MASS J2234, 2MASS J1553 and 2MASS J0335 are accreting T Tauri stars while 2MASS J0557 probably is as well. The corresponding age limit for each of these objects (again top left to bottom right) is \sim 1 (Allers et al., in press), 3 (White & Basri 2003), 10, 10 (Barrado y Navascués & Martín 2003), and 300 Myr, with the standard star GJ 406 likely > 1 Gyr.